SCK•CEN
STUDIECENTRUM VOOR KERNENERGIE
CENTRE D'ÉTUDE DE L'ÉNERGIE NUCLÉAIRE

Fracture toughness evaluation of circumferentially-cracked round bars

M. Scibetta
SCK•CEN, Mol, Belgium

01-05-1996

BLG-716

Fracture toughness evaluation of circumferentially-cracked round bars

M. Scibetta
SCK•CEN, Mol, Belgium

01-05-1996

BLG-716

Fracture toughness evaluation of circumferentially-cracked round bars

Abstract

The measure of the fracture toughness of a circumferentially-cracked round bar is generally performed through approximate formulae. Comparison of existing formulae to finite element results does not always show good agreement. Therefore an eta factor (η) is introduced in order to improve the existing analytical formula.

The axisymmetrical geometry is generally considered to be a high constrained geometry. Finite element calculations are performed to verify and quantify the constraint relative to the three point bending configuration (precracked Charpy).

1 Introduction

Mechanical properties of reactor pressure vessel steels are subject to degradation caused by neutron irradiation and thermal ageing. Safety and reliability of nuclear power plants depend largely on monitoring of the material properties through evaluation of tests on surveillance specimens. The transition temperature shift obtained from the Charpy impact test is used to evaluate the fracture behaviour through semi-empirical correlations, that are mainly based on a large experimental database. Sometimes, this results in large conservatism penalizing the operation of some reactors. Therefore, direct fracture toughness measurements are desirable. As a consequence, the application of the three-point bending technique to Charpy-size samples has been thoroughly investigated. However, this technique suffers from the complexity of the method together with a large scatter due to specimen size and loss of constraint. Another important aspect for the investigation of the radiation damage of materials is to use miniaturized samples, as the amount of irradiated material available is generally very limited. The precracked tensile bar seems very promising to address both aspects, i. e. fracture toughness measurements to monitor the transition temperature shift as well as the implications of fracture toughness parameters derived from miniaturised samples to assess radiation damage.

In this report, the determination of the best analytical formula that allows to evaluate the fracture toughness of a circumferentially-cracked round bar is examined in detail.

2 Fracture toughness

2.1 Linear elastic fracture mechanics (LEFM)

A fracture toughness measurement consists in testing a precracked specimen. The displacement versus load is recorded and used to derive the fracture toughness. The procedure is well established and described in the E339 ASTM standard [AST-90] for various specimens and test configurations. Here, the domain of validity of the linear fracture mechanics for the circumferentially-cracked round bar is investigated and compared to the standard specimen.

The stress intensity factor for the circumferentially-cracked round bar is established by Benthem and Koiter [BEN-73]:

$$K = G\left(\frac{a}{b}\right)\,\sigma\,\sqrt{\pi a(1 - a/b)} \quad \text{with} \quad \sigma = \frac{P}{\pi a^2} \tag{1}$$

$$\text{and} \quad G\left(\frac{a}{b}\right) = \frac{1}{2}\left[1 + \frac{1}{2}\left(\frac{a}{b}\right) + \frac{3}{8}\left(\frac{a}{b}\right)^2 - 0.363\left(\frac{a}{b}\right)^3 + 0.731\left(\frac{a}{b}\right)^4\right] \tag{2}$$

where P is the tensile load, 2a the ligament diameter and 2b the bar diameter (see Figure 1).

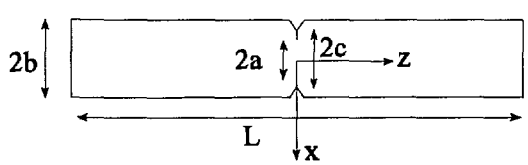

Figure 1 : *Geometry of the circumferentially-cracked round bar*

If the load is proportional to the displacement until fracture of the specimen occurs, then linear elastic fracture mechanics can be used. In this case, the fracture toughness that characterises the material corresponds to the maximal stress intensity factor. But, this situation occurs for a low fracture toughness and a large specimen.

A validity condition established experimentally [SHE-82] is formulated for a/b in the range of $0.4<a/b<0.6$:

$$2b \geq 1.5\left(\frac{K_{Ic}}{\sigma_0}\right)^2 \tag{3}$$

where K_{Ic} is the fracture toughness of the tested material and σ_0 the yield stress.
For a = 0.5 b the condition becomes:

$$a \geq 0.375\left(\frac{K_{Ic}}{\sigma_0}\right)^2 \tag{4}$$

Based on other experimental results, Lucon [LUC-92] suggests:

$$a \geq 5\, r = \frac{5}{6\pi}\left(\frac{K_{Ic}}{\sigma_0}\right)^2 = 0.265\left(\frac{K_{Ic}}{\sigma_0}\right)^2 \tag{5}$$

where r is the plastic zone size.

Ibrahim [IBA-87] suggests two conditions based on finite element results:

$$c-a \geq 2\, r = \frac{2}{6\pi}\left(\frac{K_{Ic}}{\sigma_0}\right)^2 \tag{6}$$

where 2c is the initial ligament diameter and c-a is the fatigue crack length.

For a = 0.5 b and c=0.7 b the condition is:

$$a \geq 0.265\left(\frac{K_{Ic}}{\sigma_0}\right)^2 \tag{7}$$

He also proposes an additional condition to avoid general yielding of the ligament:

$$2.5\ \sigma_0 \geq \sigma \tag{8}$$

where σ is the average stress across the ligament.

For a = 0.5 b using Benthem stress intensity function [BEN-73], the condition becomes:

$$a \geq 0.36\left(\frac{K_{Ic}}{\sigma_0}\right)^2 \tag{9}$$

All equations (Equation 3, 5, 6 and 8) give similar conditions to measure the fracture toughness in the range of $0.4 < a/b < 0.6$. The most severe condition is obtained from Equation 3:

$$a \geq 0.375\left(\frac{K_{Ic}}{\sigma_0}\right)^2 \tag{10}$$

Nevertheless the size requirement condition is 6.7 times less severe than with standard specimen [AST-90] allowing the use of smaller specimens:

$$\text{ASTM:}\quad a, B \geq 2.5\left(\frac{K_{Ic}}{\sigma_0}\right)^2 \tag{11}$$

where B is the thickness, and a the crack length of three-point bend or compact tension specimen.

To avoid perturbation on the measured fracture toughness due to fatigue precracking, the maximal stress intensity factor during precracking should not exceed 60% of the fracture toughness [LUC-90, AST-90].

$$K_f < 0.6\ K_{Ic} \tag{12}$$

To summarise, different authors established experimentally or numerically the domain of valid elastic fracture toughness measurement. All authors agree fairly well in the range of interest $0.4<a/b<0.6$. The established condition is 6 times less severe than with standard bending specimens.

2.2 Elastic plastic fracture mechanics (EPFM)

When the load versus displacement displays a non-linear behaviour, the fracture toughness is measured through the J-integral introduced by Rice [RIC-68a].

The J-integral [RIC-68a] for a 2D crack is:

$$J = \int_{\Gamma} W n_1 - \sigma_{ij}\, n_j\, \partial_i u_1 \, d\Gamma \qquad \text{with} \qquad W = \int_0^t \sigma_{ij}\, \dot{e}_{ij}\, dt \tag{13}$$

where W is the energy density, Γ is a path around the crack and the crack lips are oriented along the x_1 axis (see Figure 2).

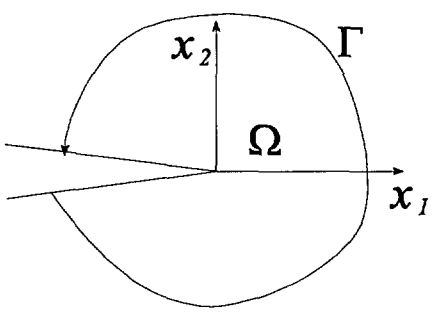

Figure 2 : *Local axis for J-integral evaluation*

For axisymmetric situations, a surface integral must be taken into account [BER-77]. The J-integral is given by:

$$J = \int_{\Gamma} (W n_1 - \sigma_{ij}\, n_j\, \partial_i u_1)\, \frac{r}{a}\, d\Gamma + q \int_{\Omega} (\sigma_3\, e_3 - W)\, d\Omega \tag{14}$$

where q = +1 for internal crack and -1 for external crack, all quantities are expressed in local axis (see Figure 2) and Ω is the area delimited by Γ.

Broberg [BRO-76] derived another expression for axial symmetry:

$$J = \int_{\Gamma} (W n_1 - \sigma_{ij}\, n_j\, \partial_i u_1)\, d\Gamma + q \int_{\Omega} (\sigma_3\, e_3 - \sigma_1\, e_1 - \sigma_{12}\, \partial_1 u_2)\, d\Omega \tag{15}$$

The SYSTUS code uses a path integral expression [BUD-73, MUD-82] for power law hardening material:

$$J = \int_{\Gamma} \left[(W n_1 - \sigma_{ij}\, n_j\, \partial_i u_1)\, \frac{r}{a} + (W n_2 - \sigma_{ij}\, n_j\, \partial_i u_2)\, \frac{z}{a} - \left(\frac{3}{n} - 1\right) \sigma_{ij}\, n_j\, u_i \right] \frac{r}{a}\, d\Gamma \tag{16}$$

The J-integral is demonstrated [RIC-68a] to be path independent under three hypotheses:

- small strain model

The small strain model is considered valid if the strain is less than 10% [AND-95]. This condition is never fulfilled at the crack front due to blunting of the crack. The size of this large strain zone is

about the Crack Tip Opening Displacement CTOD (see Figure 3). If this zone is small compared to the ligament, it can be neglected.

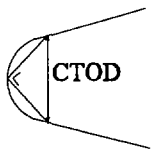

Figure 3 : *Crack Tip Opening Displacement CTOD*

- a plastic potential function describes the material behaviour

This potential function allows a unique relation between stress and strain:

$$\sigma_{ij} = \frac{\partial W}{\partial e_{ij}} \tag{17}$$

This potential function exists for any elastic plastic material (incremental theory with Von Mises criterion) if proportional loading (i.e. stress components changing in fixed proportion to one another) occurs everywhere [HUT-83].

An easy way to verify the proportional loading condition is to plot the stress versus a dimensionless distance:

$$\frac{\sigma_{ij}}{\sigma_0} = f_{ij}\left(\frac{r\sigma_0}{J}\right) \tag{18}$$

where σ_0 is the yield stress of the material.

If the f_{ij} function is independent of the load level, the proportional loading condition is satisfied. In this case, J univocally defines crack tip stress and strain. When a loss of constraint is observed, other parameters such as T stress or Q factor [AND-95] should be introduced to characterise the stress field.

- no local unloading occurs

No local elastic unloading is accepted. An elastic unloading typically occurs as a consequence of crack extension. If the unloading zone is limited, the J-integral can also control crack extension [AND-95].

If the three former conditions are satisfied, and if the size of the microscopic process of fracture is smaller than the zone controlled by the small strain solution, the J-integral at initiation (J_c) is a valid measure of the fracture toughness [HUT-83].

The J-integral is consequently path independent for an elastic material. In plane strain condition, the relation between the stress intensity factor and the J-integral is [AND-95]:

$$K_J = \sqrt{\frac{J\,E}{1 - \nu^2}} \tag{19}$$

2.3 Approximate formulae for J

Different authors [RIC-73, ITO-88, BER-81, NEA-95] proposed different expressions to link the J-integral to measured load and displacement for circumferentially-cracked round bars. Although approximate, these analytical expressions are of first importance to experimentally evaluate the J-integral.

Four different formulations found in the literature are presented here.

The total displacement is generally splited into different part:

- elastic and plastic term:

$$\delta = \delta_e + \delta_{pl.} \tag{20}$$

- displacement due to the crack and without crack:

$$\delta = \delta_c + \delta_{n.c.} \tag{21}$$

1) Rice [RIC-73] established a J formula for deep crack using dimensionless relations:

$$J = \frac{1}{2\pi a^2}\left[3\int_0^{\delta_c} P\, d\delta_c - P\delta_c\right] \tag{22}$$

where 2a is the ligament diameter and δ_c the displacement due to the crack

2) Itoh [ITO-88] derived from Equation 22 another equivalent expression:

$$J = \frac{K_I^2(1-\nu^2)}{E} + \frac{1}{2\pi a^2}\left[3\int_0^{\delta} P\, d\delta - P\delta - \frac{P\delta_e}{2}\right] \tag{23}$$

where δ is the total displacement, δ_e the elastic part of the displacement and K_I the stress intensity factor for this geometry under load P.

For a shallow crack and using dimensionless relations, he found:

$$J = \frac{1}{2\pi a(b-a)}\left[\int_0^{P} \delta\, dP - \frac{P\delta_{n.c.}}{2}\right] \tag{24}$$

where $\delta_{n.c.}$ is the elastic displacement without crack.

3) Based on finite element calculation, Beremin [BER-81] found:

$$J = \frac{K_I^2(1-\nu^2)}{E} + \frac{P\,\delta_{pl.}}{2\pi a^2} \tag{25}$$

where $\delta_{pl.}$ is the plastic part of the displacement.

4) Based on limit load function for this geometry, Neale [NEA-95] derived:

$$J = \frac{K_I^2(1-\nu^2)}{E} + \frac{\int_0^{\delta_{pl.}} P \, d\delta_{pl.}}{2\pi a^2} \qquad \text{for a/b} > 0.35 \tag{26}$$

$$J = \frac{K_I^2(1-\nu^2)}{E} + \frac{\int_0^{\delta_{pl.}} P \, d\delta_{pl.}}{\pi a^2} \qquad \text{for a/b} < 0.35 \tag{27}$$

In conclusion, the accuracy and the domain of validity of the submentioned formulations are not clear. To compare the different relations a force displacement curve is needed and can be obtained using numerical or experimental simulations. To evaluate the accuracy of the different formulae, direct use of the definition (Equation 13) is the only possibility. This definition requires the knowledge of the stress and strain field given by analytical or numerical results.

2.4 Finite element calculations

The goal is to obtain the best analytical formulation for the J-integral of a circumferentially-cracked round bar and to quantify the accuracy of the different approximate formulae as proposed in the literature. The material behaviour law, the a/b ratio and the load level are the three parameters governing the problem. Each of them is studied separately.

2.4.1 Material behaviour law

The material behaviour modifies the load displacement curve and consequently the J-integral. The study is limited to the very popular material model namely: isotropic strain-hardening based on the Von Mises criterion. To describe the true stress-strain curve of a uniaxial test, a power law is used:

$$\frac{\sigma}{\sigma_0} = \begin{cases} \dfrac{\varepsilon}{\varepsilon_0} & \text{if} \quad \sigma < \sigma_0 \\ \left(\dfrac{\varepsilon}{\varepsilon_0}\right)^n & \text{if} \quad \sigma \geq \sigma_0 \end{cases} \tag{28}$$

with

$$E\,\varepsilon_0 = \sigma_0 \tag{29}$$

where E is the Young modulus, σ the true uniaxial stress, ε the true uniaxial strain, σ_0 the yield stress and n the strain hardening exponent ($n < 1$).

2.4.2 The strain hardening exponent

Three different strain hardening exponents (see Figure 4) were chosen for a fixed ratio $E/\sigma_0=410$. Young modulus is 205000 MPa, and the Poisson ratio is fixed to $\nu=0.3$.

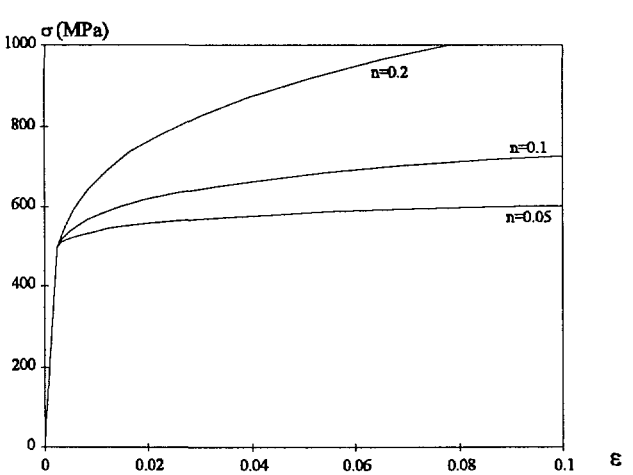

Figure 4 : *True uniaxial stress versus strain (E = 205000 MPa, σ_0 = 500 MPa)*

To study the effect of the strain hardening exponent, the selected geometry (see Figure 1) has the following dimensions:

- the diameter 2b = 10 mm,
- the ratio a/b = 0.5,
- the ratio L/b=11.

The different analyses are performed with a rather coarse mesh (see Figure 5) using 8-nodes axisymmetric isoparametric elements, as no strong effect of the mesh was observed.

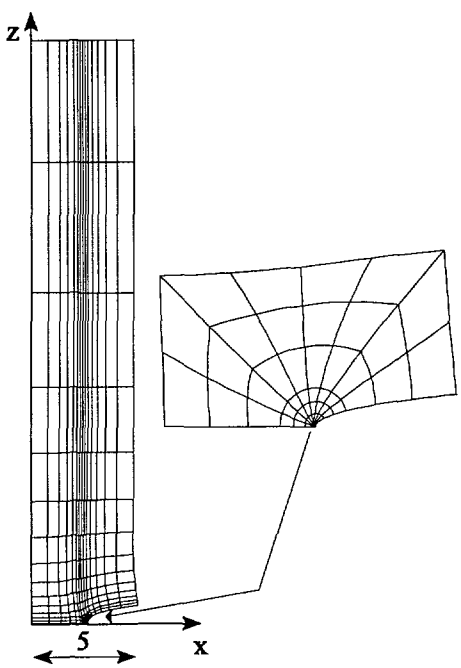

Figure 5 : *Deformed mesh a/b=0.5*

Both large and small strain models were used to obtain the load displacement curve, but no significant differences were found (less than 5%). This observation can be explained by the fact that region of strains greater than 10% is limited to a small area ahead of the crack front.

For n = 0.1 and a/b = 0.5, a fixed displacement of 0.4 mm is imposed, at which J is equal to 250 kJ/m^2 and the Crack Tip Opening Displacement (CTOD) equals 220μm. The area where the strain is greater than 10% corresponds to 0.1064 mm^2. The square root of this surface yields a typical distance of 326 μm. This distance is of the same magnitude as the CTOD and is 7.7 times smaller than the initial ligament (2500 μm).

Figure 6 shows a strong dependence of the strain hardening exponent on the load displacement curve at high load levels. It is also important to notice that specimens are loaded well beyond the small scale yielding, as the plastic zone can be as large as the bar diameter (see Figure 7).

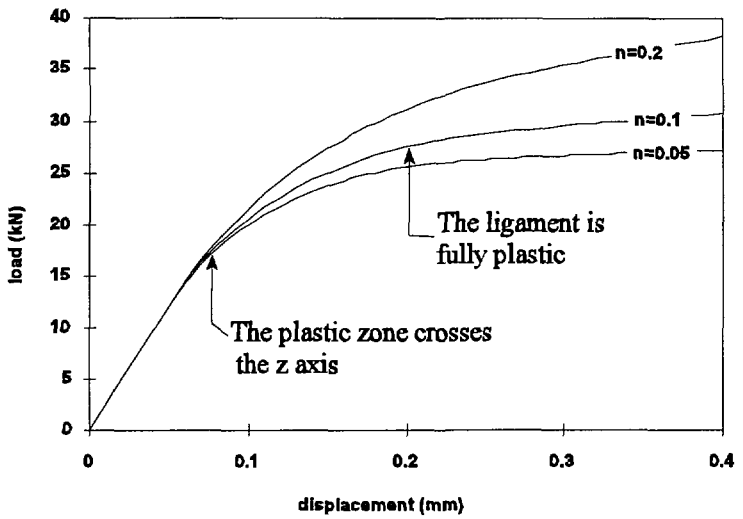

Figure 6 : *Load displacement curve (a/b =0.5, E/σ_0=410)*

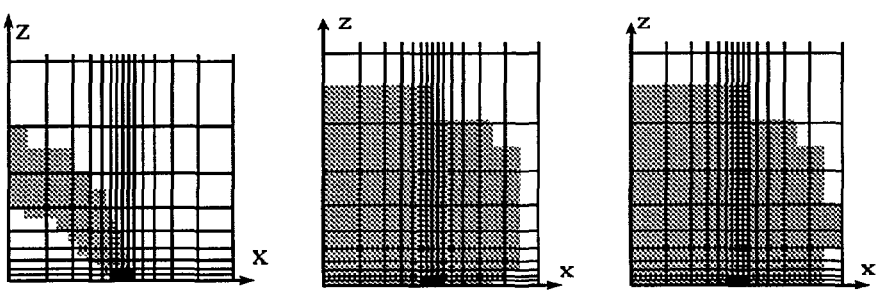

a) displ.=0.07 mm *b) displ.=0.2 mm* *c) displ.=0.21 mm*

Figure 7 : *Plastic zone shape (a/b =0.5, n=0.1, E/σ_0=410)*

The J-integral increases with displacement. This quantity is calculated numerically for different hardening exponents using the Equivalent Domain Integral (EDI). The choice of this method is explained in Paragraph 2.5.

Figure 8 shows only a very weak effect of the hardening exponent on the J-integral. This is unexpected as the hardening exponent largely affects the load-displacement curve.

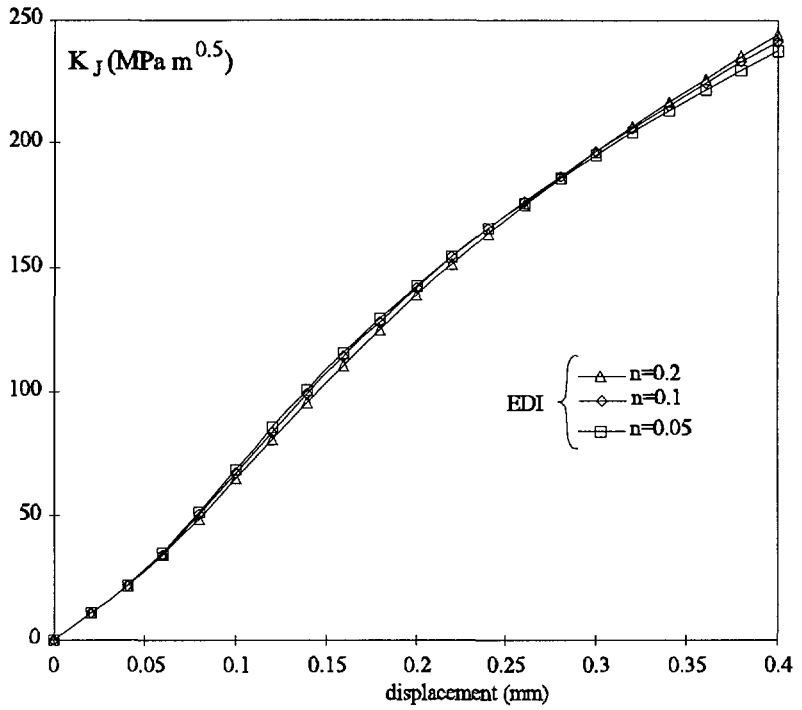

Figure 8 : *K_J obtained by the Equivalent Domain Integral (a/b =0.5, E/σ_0=410)*

The different analytical formulae are compared with the finite element calculation Figures 9 to 13. As no significant effect of the hardening exponent is observed for the finite element solution, it is only plotted for n=0.1.

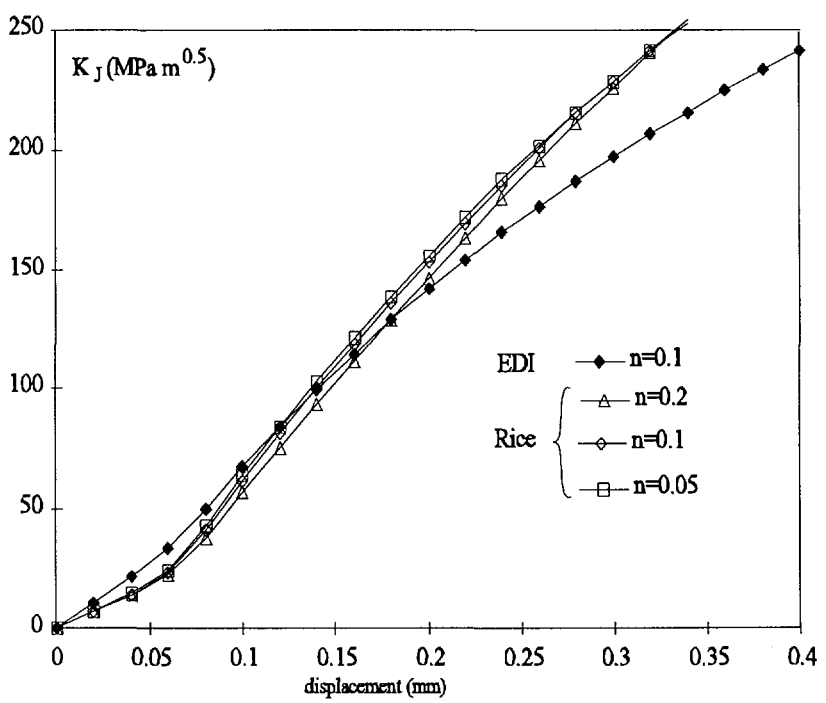

Figure 9 : *K_J compared with Equation 22 (a/b =0.5, E/σ_0=410)*

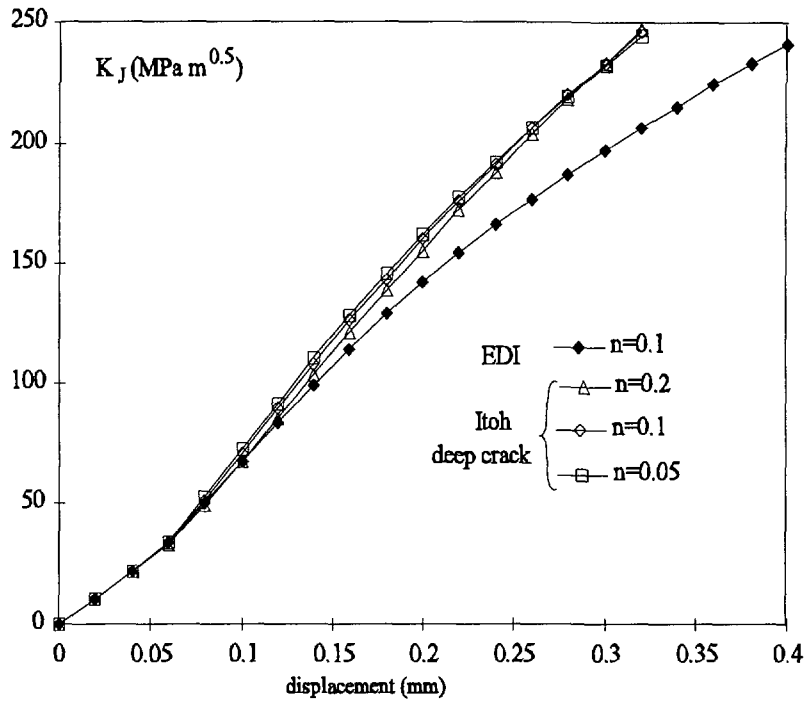

Figure 10 : *K_J compared with Equation 23 (a/b =0.5, E/σ_0=410)*

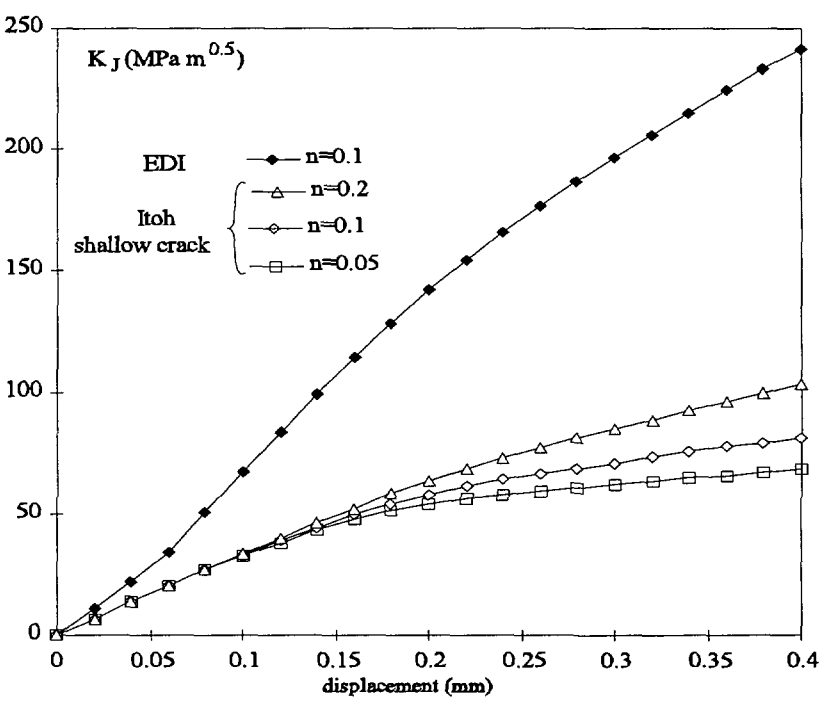

Figure 11 : *K_J compared with Equation 24 (a/b =0.5, E/σ_0=410)*

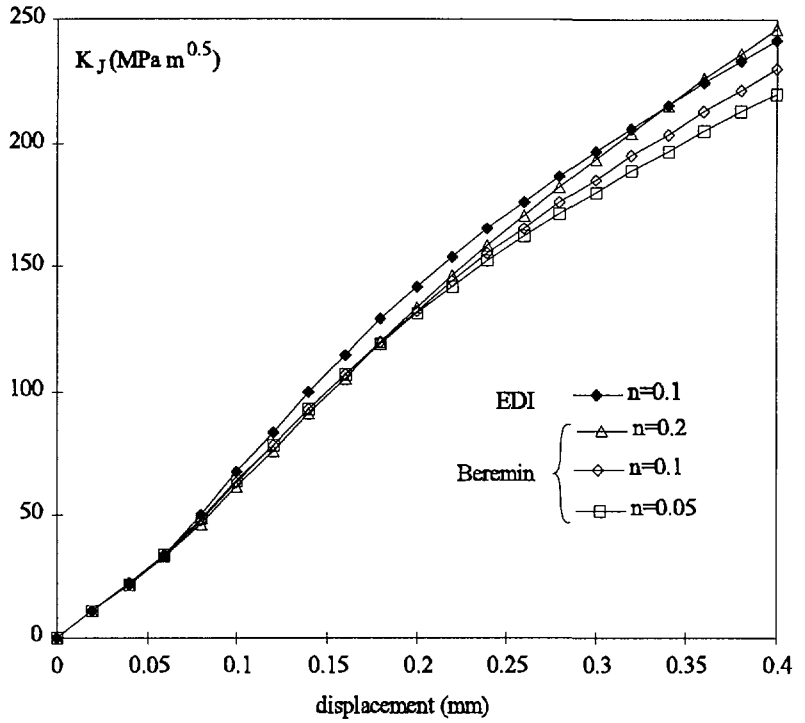

Figure 12 : *K_J compared with Equation 25 (a/b =0.5, E/σ_0=410)*

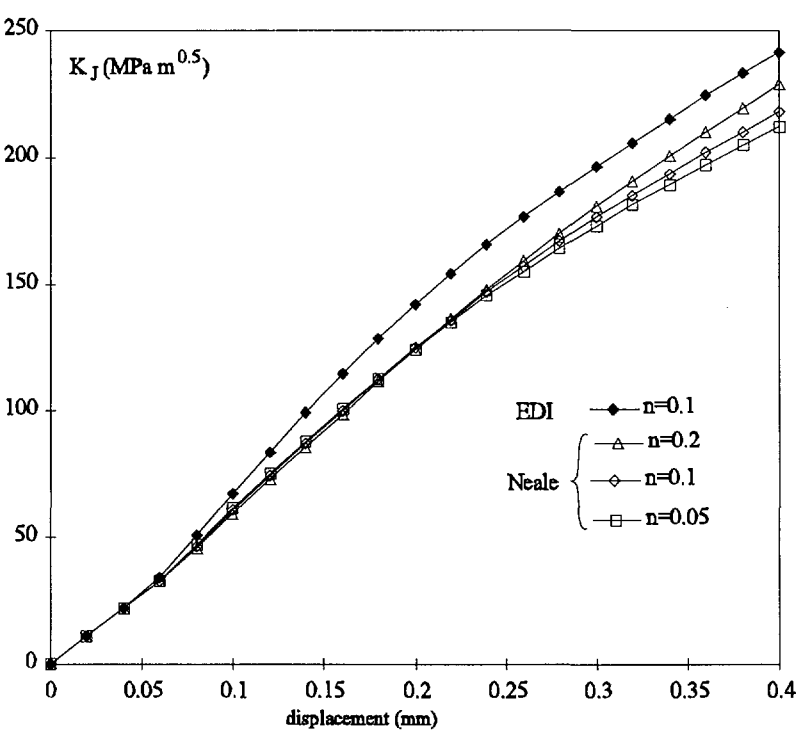

Figure 13 : *K_J compared with Equation 26 (a/b =0.5, E/σ_0=410)*

Discussion:

In the examinated range, all approximate formulae (except Itoh shallow crack) do not show a strong influence of the hardening exponent on the J-integral, confirming the finite element results.

Concerning the accuracy of the different formulae, Rice and Itoh's formulations for deep crack overestimate the J-integral. The domain of validity of this two formulae certainly allows larger precrack (a/b<0.5). Itoh formulation for deep crack is more accurate than Rice for low load, as elastic effects are decoupled.

Beremin and Neale's equations are the most accurate for a/b=0.5. But Neale's equation is preferred as it is based on analytical considerations.

Itoh equation for shallow crack largely underestimates the J-integral. The domain of validity is thus well beyond a/b>0.5.

2.4.3 The yield stress

Analyses for 3 different E/σ_0 ratios (n=0.1, a/b=0.5) are also performed to study the effect of the yield stress. Figure 14 shows the force displacement curve and the J-integral is plotted in Figure 15.

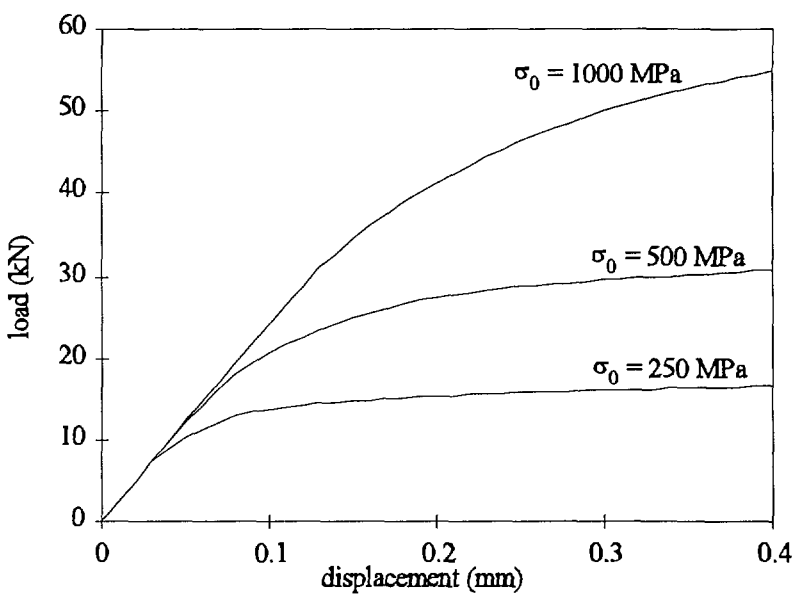

Figure 14 : *Load displacement curve for different yield stress (n=0.1, a/b =0.5, E=205 GPa)*

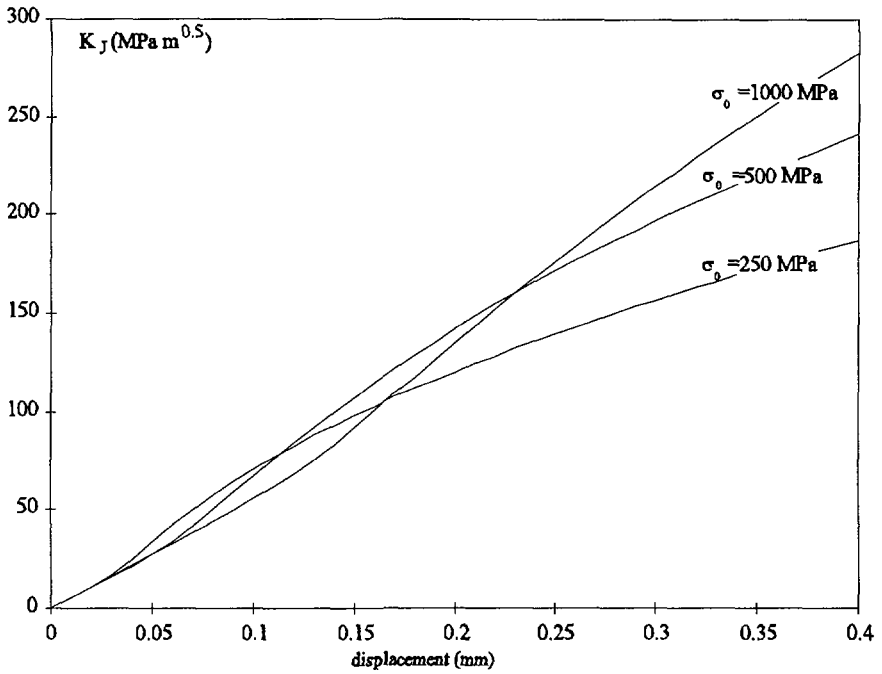

Figure 15 : *Effect of yield on K_J (n=0.1, a/b =0.5)*

The yield stress drastically affects the load displacement curve (Figure 14) and also affects the J-integral.

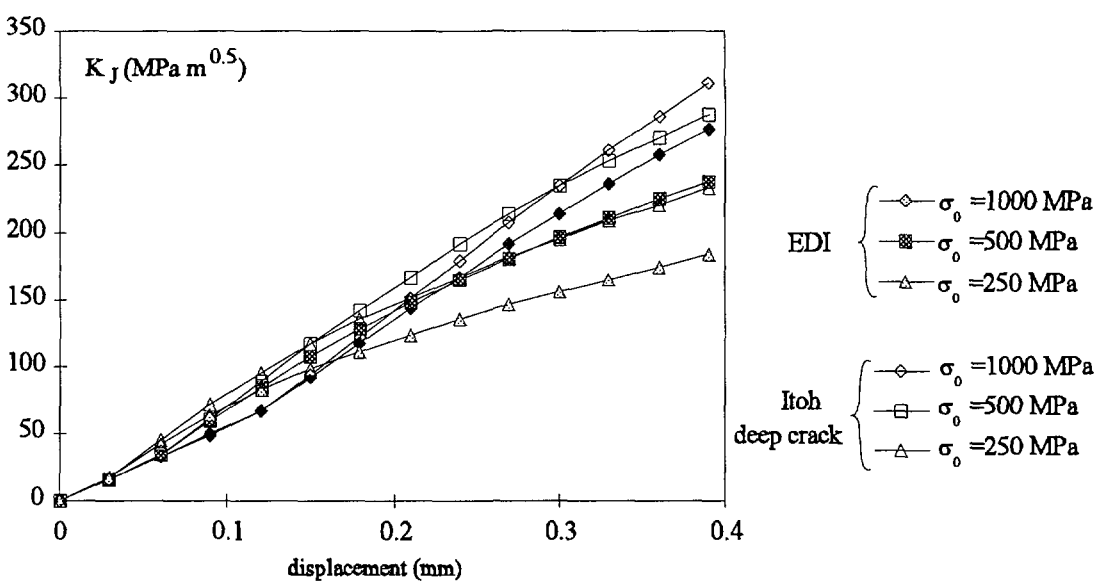

Figure 16 : *K_J compared with Equation 23 (a/b =0.5, n=0.1)*

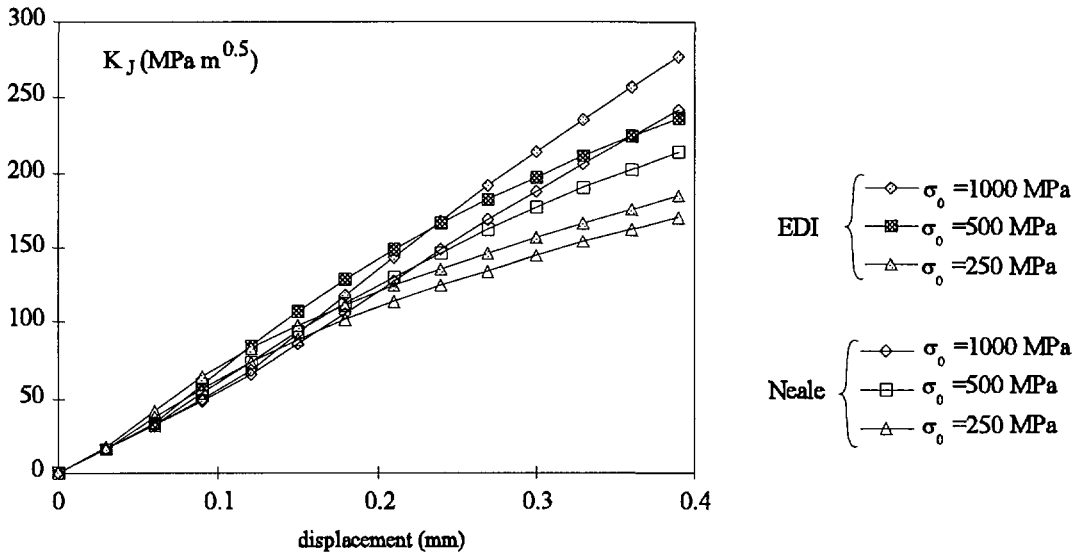

Figure 17 : *K_J compared with Equation 26 (a/b =0.5, n=0.1)*

Discussion:

Figures 16 and 17 show the comparison of the J-integral calculated using analytical formulae for different yield stresses. Each analytical formula predicts a higher value of the J-integral for a higher yield stress. The accuracy of each formulation dependent on the yield stress.

Figures 16 and 17 also show the complexity and the difficulty to correct Equation 21 or 24 to take the yield stress into account.

2.4.4 The a/b ratio

To isolate the effect of the a/b ratio, analyses are performed with a fixed value of the hardening exponent (n=0.1) and a fixed ratio $E/\sigma_0 = 410$.

Figure 18 shows the load displacement curves for different a/b ratios. It also gives some useful indications on the plastic zone size (see also Figures 19 and 20). As expected, the limit load increases with higher a/b ratio.

For large ligaments (a/b>0.6), the plasticity reaches the external surface (see Figure 18) before the complete plastification of the ligament. This results in a loss of triaxiality and constraint, inducing the loss of J-integral dominance.

For small ligaments (a/b<0.3), the deformation of the ligament is rather large. This large deformation in the blunting zone can also lead to a loss of constraint.

The optimum ratio a/b to measure high fracture toughness without loss of triaxiality is certainly in the range of 0.3<a/b<0.6.

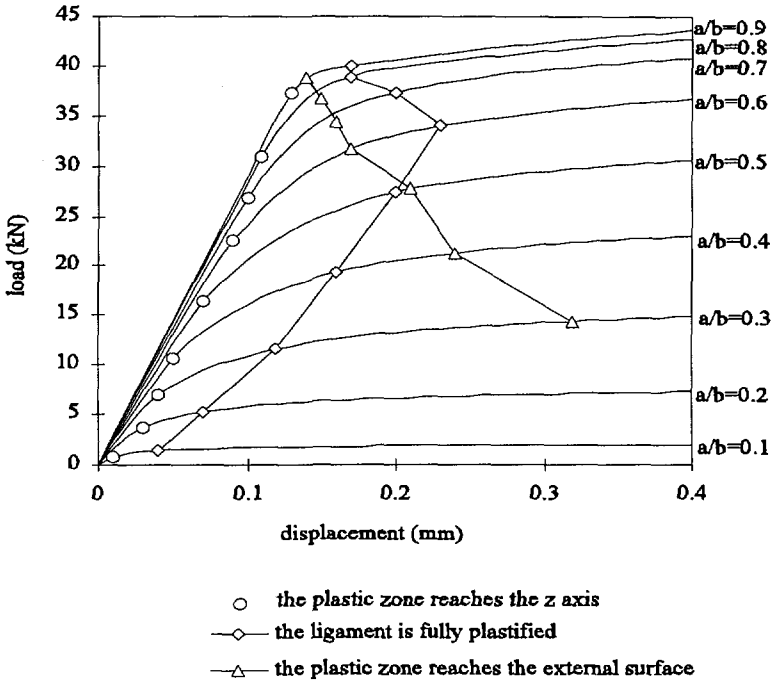

Figure 18 : *Force displacement curve for different a/b ratio ($n=0.1$, $E/\sigma_0=410$)*

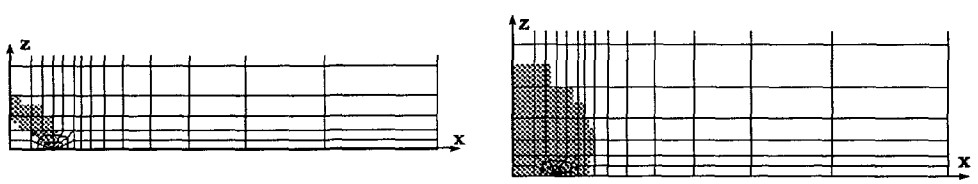

a) displ.=0.01 mm *b) displ.=0.04 mm*

Figure 19 : *Plastic zone shape ($a/b=0.1$, $n=0.1$, $E/\sigma_0=410$)*

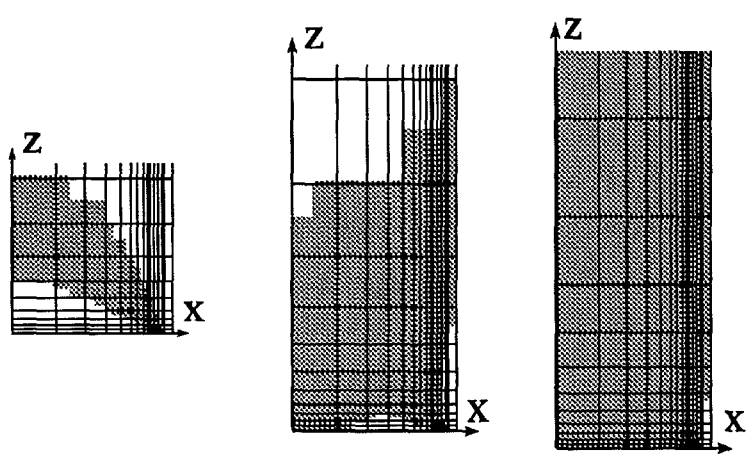

a) displ.=0.13 mm *b) displ.=0.14 mm* *c) displ.=0.17 mm*

Figure 20 : *Plastic zone shape ($a/b=0.9$, $n=0.1$, $E/\sigma_0=410$)*

Figure 21 shows the evolution of the plastic zone size and the J-integral calculated using the Equivalent Domain Integral. Under the hypothesis that the plastification of the ligament or the complete section introduces a loss of constraint and consequently unreliable fracture toughness measurements, the optimum value of the a/b ratio is about 0.45. However, in the range of $0.3<a/b<0.55$, the geometry is still highly constrained.

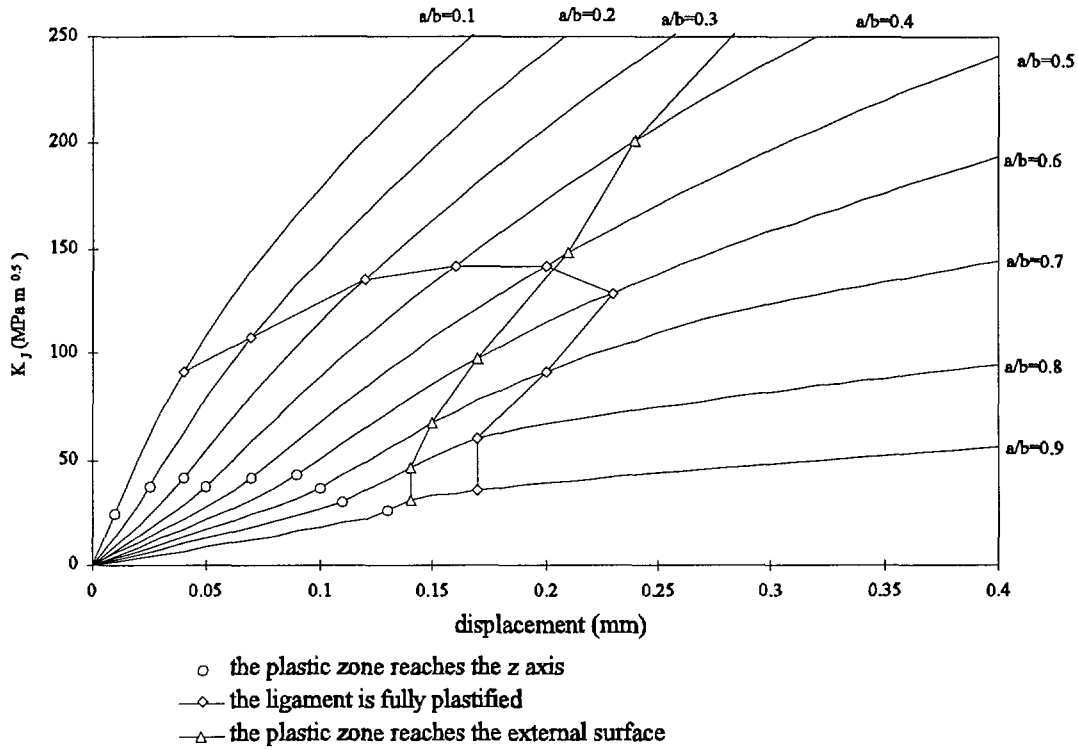

Figure 21 : *Effect of the ligament size on the J-integral ($n=0.1$, $E/\sigma_0=410$)*

For various a/b ratios, different approximate formulations of the J integral are compared with finite element results (see Figures 22 to 30).

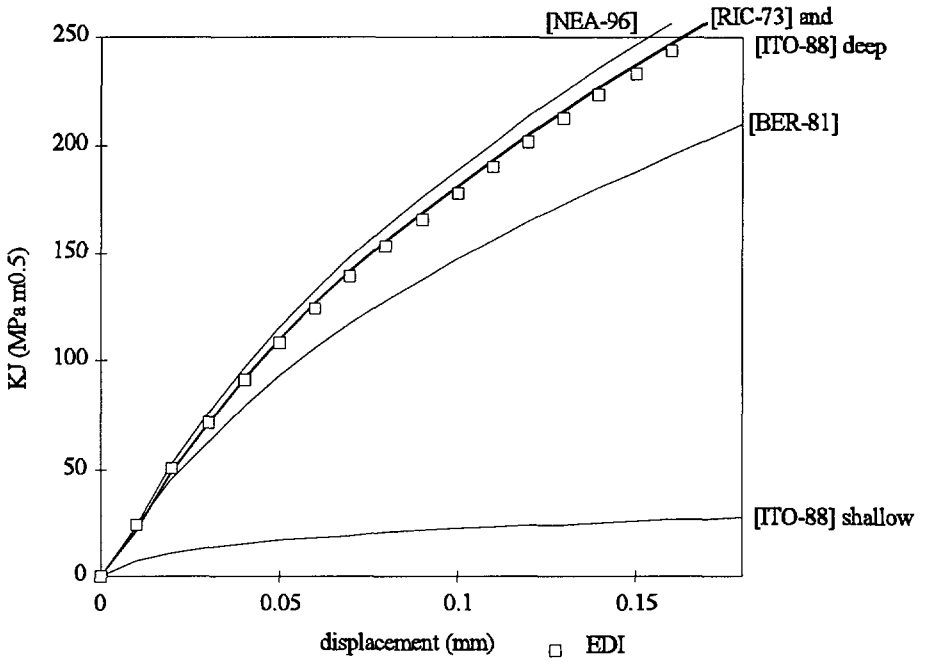

Figure 22 : *Comparison of approximate formulae and the EDI (a/b =0.1)*

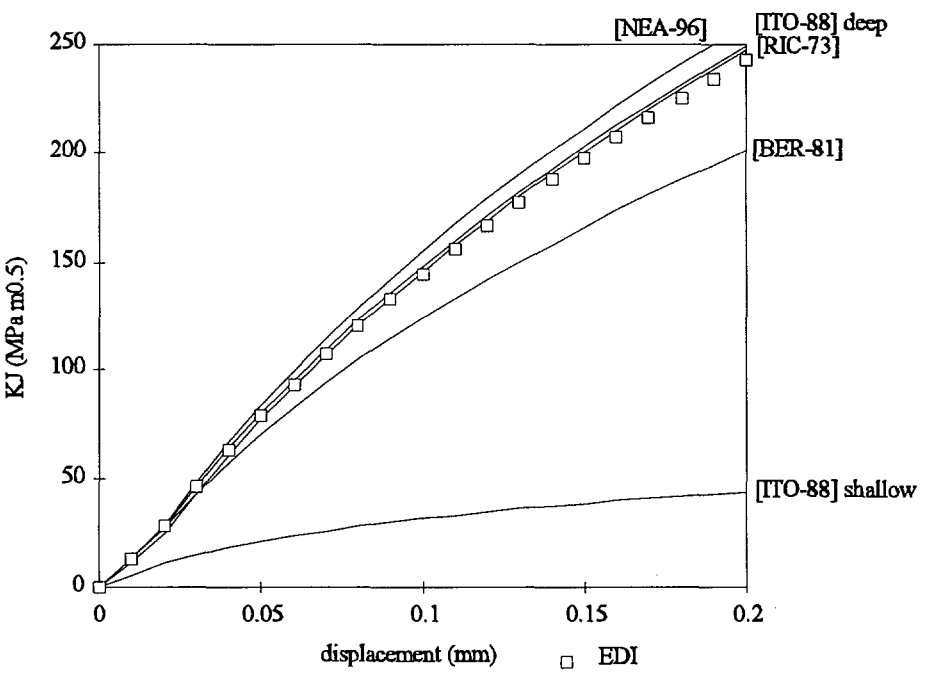

Figure 23 : *Comparison of approximate formulae and the EDI (a/b =0.2)*

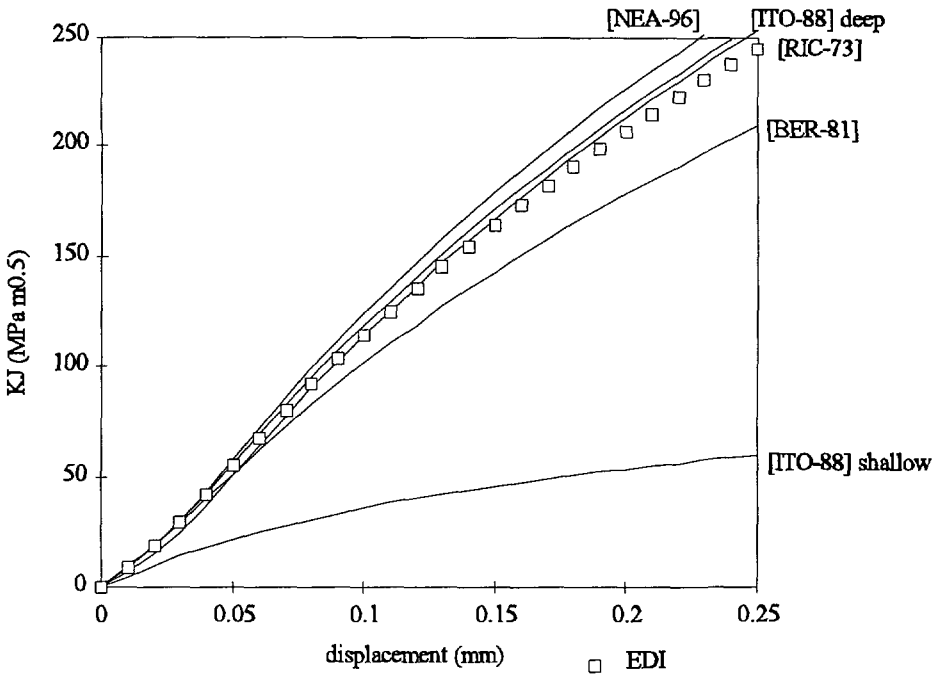

Figure 24 : *Comparison of approximate formulae and the EDI (a/b =0.3)*

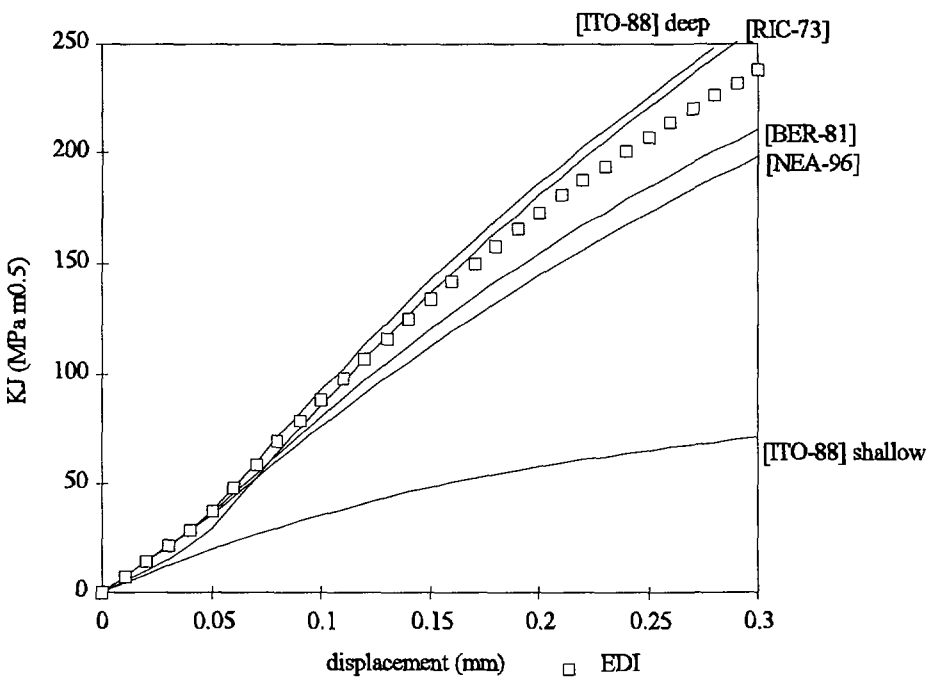

Figure 25 : *Comparison of approximate formulae and the EDI (a/b =0.4)*

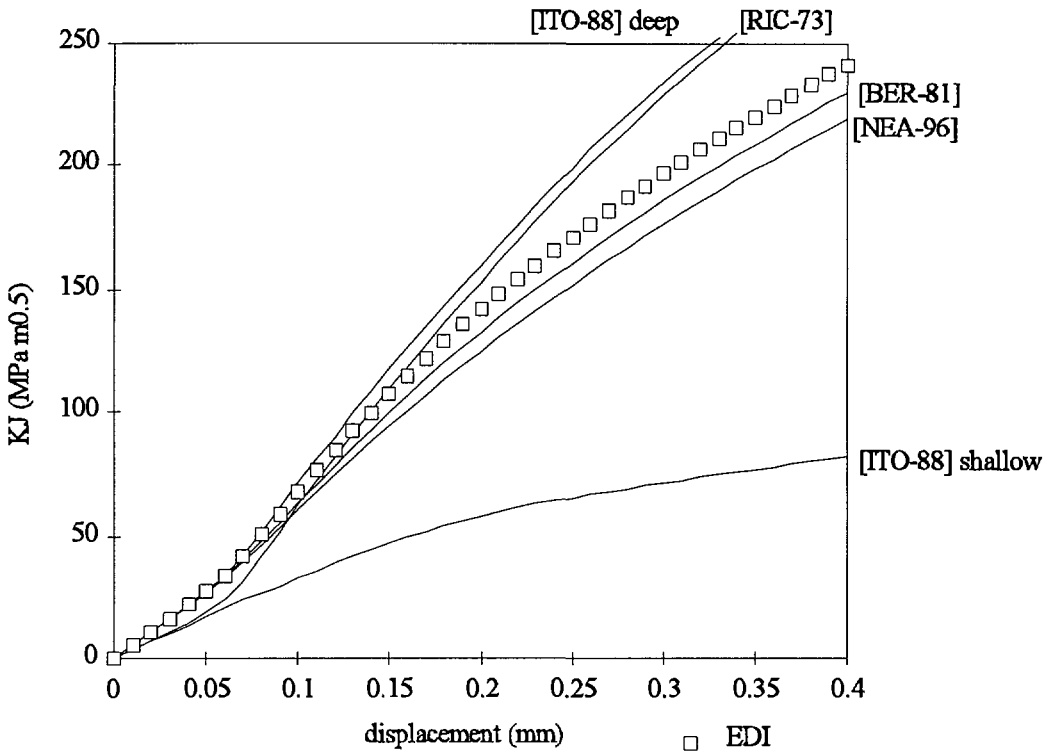

Figure 26 : *Comparison of approximate formulae and the EDI (a/b =0.5)*

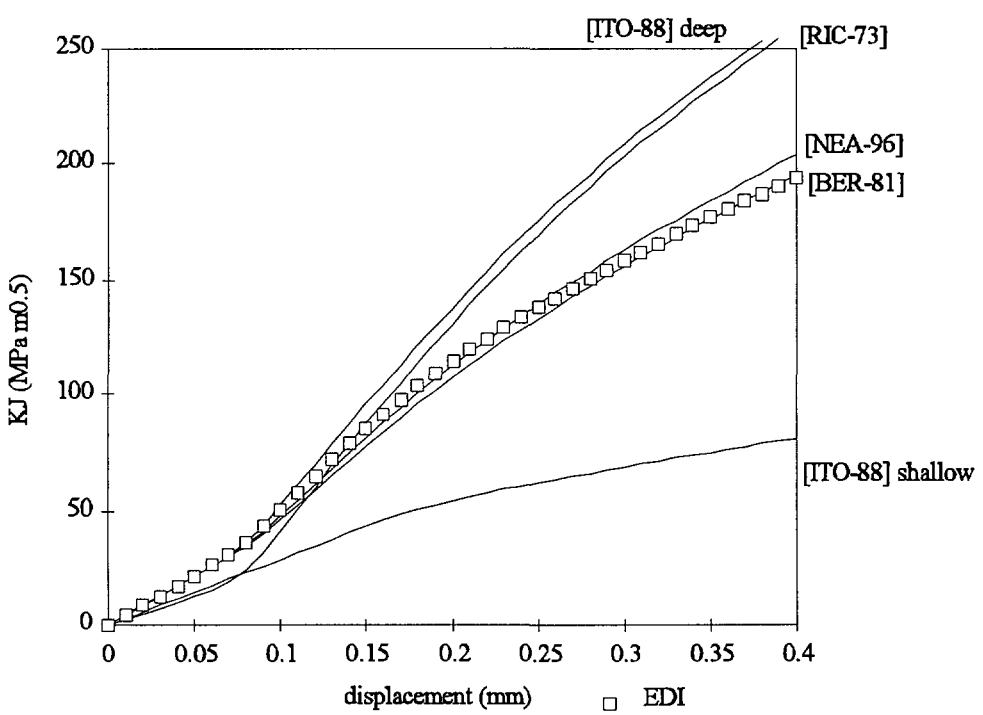

Figure 27 : *Comparison of approximate formulae and the EDI (a/b =0.6)*

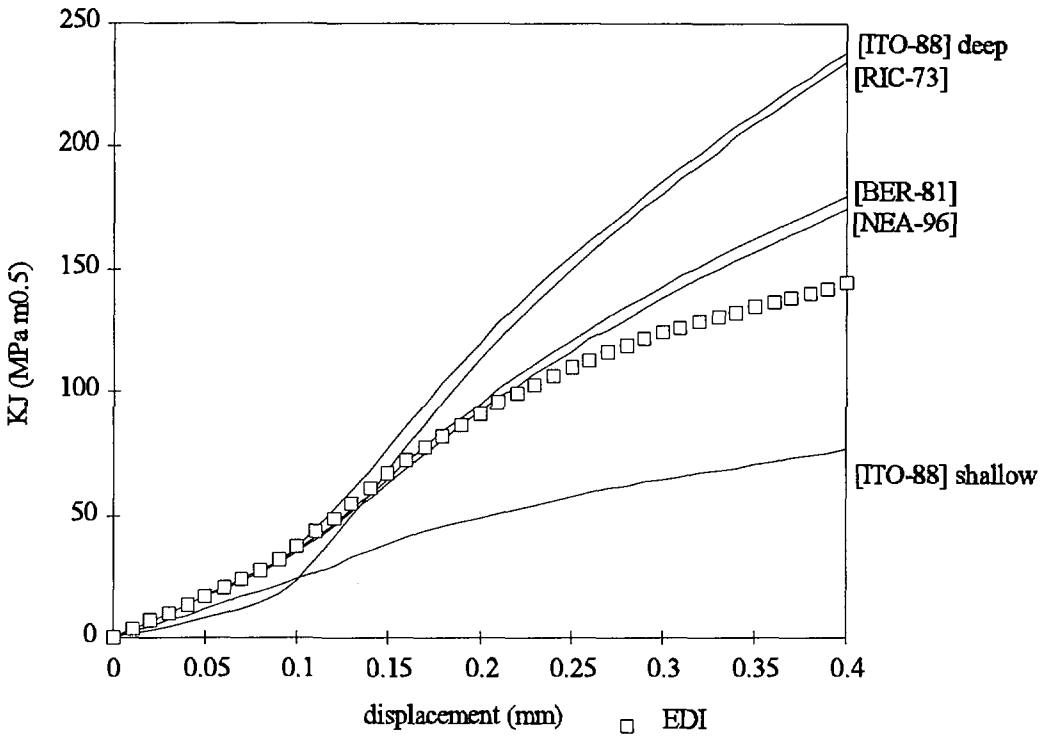

Figure 28 : *Comparison of approximate formulae and the EDI (a/b =0.7)*

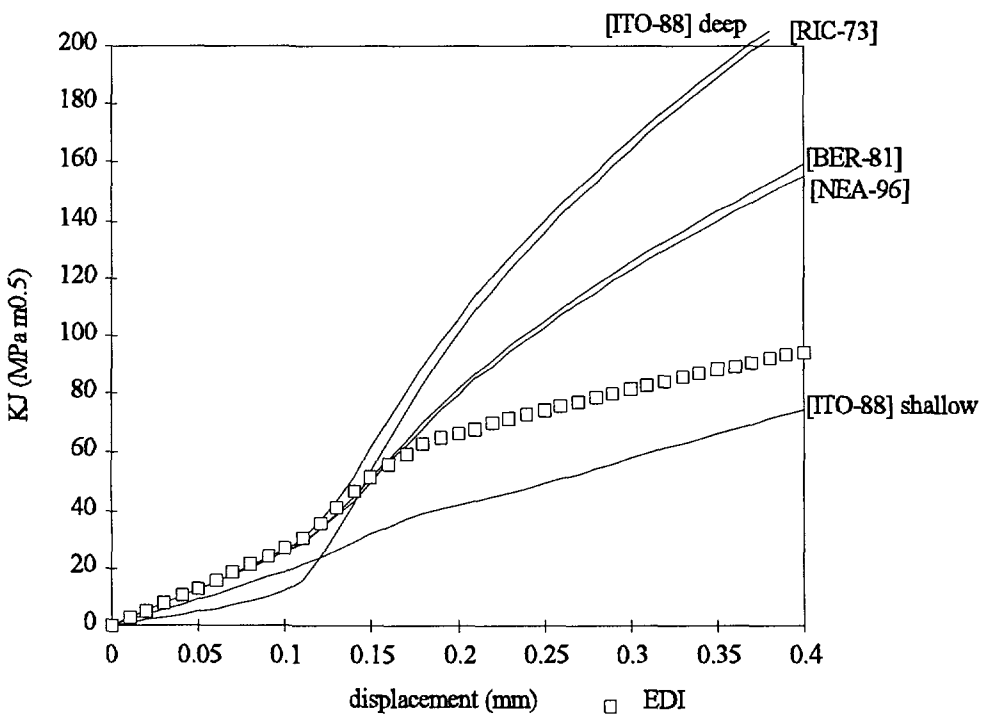

Figure 29 : *Comparison of approximate formulae and the EDI (a/b =0.8)*

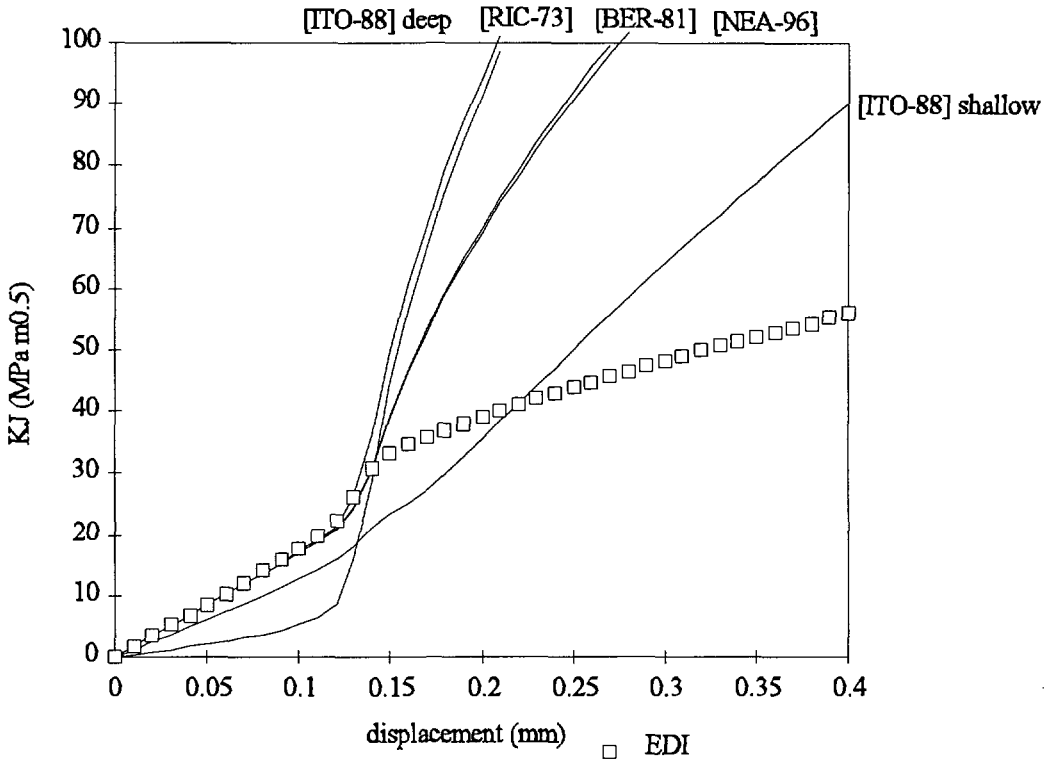

Figure 30 : *Comparison of approximate formulae and the EDI (a/b =0.9)*

Discussion:

For a/b<0.35, the recommended formulae are those of Rice and Itoh established for deep crack. Itoh's equation is slightly better for low load levels because the elastic part of the J-integral is decoupled. Neale's equation gives also good results (accuracy better than 10%).

For 0.35<a/b<0.65, Beremin and Neale's equations give approximative results (maximum 30% of difference).

For shallow crack a/b>0.65, no equation fits the results up to a specific load level.

2.4.5 The eta factor

The concept of the eta factor is largely used for compact tension and three point bending specimens and leads to very simple and reliable approximate formulae. This concept is also used by ASTM E813 standard [AST-90]. Here, the eta factor is calculated in order to study the applicability of this concept for the precracked tensile bar.

The eta factor is the ratio between the plastic part of the J-integral and the plastic energy per unit of ligament area:

$$J_{pl.} = \eta_{pl.} \frac{\int_0^{\delta_p} P \, d\delta_p}{\pi a^2} \quad \text{with} \quad J_{pl.} = J - \frac{K_I^2(1-\nu^2)}{E} \tag{30}$$

The eta factor depends on the geometry and the material and is independent of the load level under the mathematical hypothesis that the load (P) is a product of two functions. The first term take the plastic displacement into account and the second term the crack length.

$$P/(\pi a^2) = F_1(\delta_{pl.})\, F_2(a) \tag{31}$$

This relation does not exist [PAR-80] if the plastic zone shape changes due to geometrical effects.

Using the relation between the energy release rate per unit surface [AND-95] and the J-integral:

$$J_{pl.} = \int_0^{\delta_p} \left(\frac{\partial P}{2\pi a \partial a} \right)_{\delta_{pl.}} d\delta_{pl.} \tag{32}$$

the eta factor becomes:

$$\eta_{pl.} = 1 + \frac{a}{F_2} \frac{\partial F_2}{\partial a} \tag{33}$$

The case of rigid perfectly plastic materials satisfied Equation 31 [PAR-80], in this context the equation of Neale [NEA-95] was established.

$$\eta_{pl.} = 1 \quad \text{for} \quad a/b<0.35 \tag{34}$$

$$\eta_{pl.} = 0.5 \quad \text{for} \quad a/b>0.35 \tag{35}$$

For power law hardening materials and deep crack configurations, it is possible to establish a more accurate value of eta. Using Rice or Itoh's relation (Equation 22 or 23), the eta factor is:

$$\eta_{pl.} = \frac{3}{2} - \frac{1}{2} \frac{P\, \delta_{pl.}}{\int_0^{\delta_p} P \, d\delta_{pl.}} \tag{36}$$

As in the uni-axial tensile test, the load is related to the displacement by a power law:

$$P = C_0\, \delta_{pl.}^n \tag{37}$$

where n is the hardening exponent and C_0 a constant value.

The substitution of Equation 37 in 36 gives:

$$\eta_{pl.} = 1 - \frac{1}{2} n \tag{38}$$

The Neale's value for deep crack is obtained for n=0.

To obtain the eta factor for a larger range of a/b, the eta factor is computed from finite element results and presented in Figure 31.

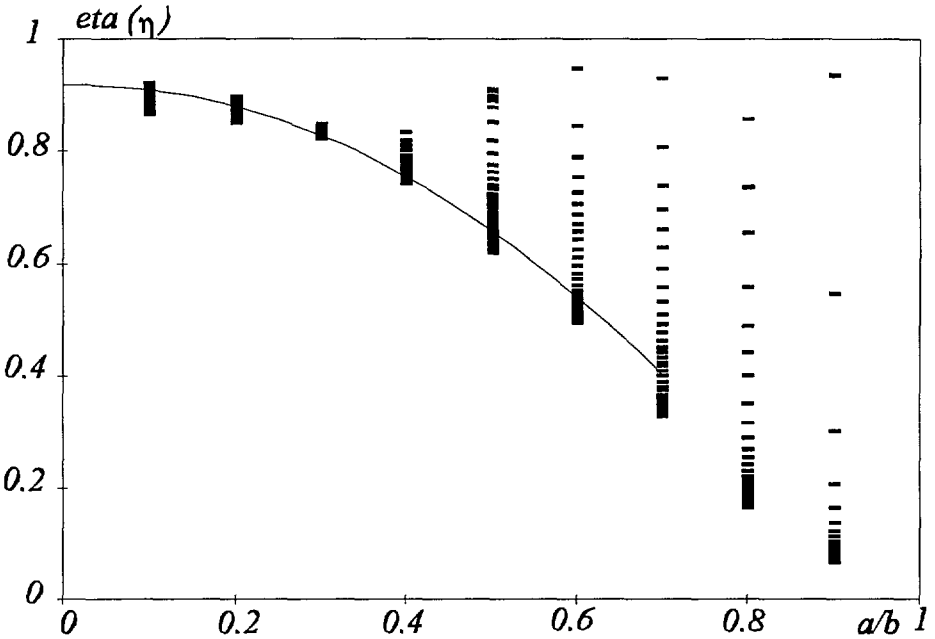

Figure 31 : *Computed eta factor for different load levels and different a/b ratio ($n=0.1$, $E/\sigma_0=410$) polynomial fit: eta =0.9165 + 0.0297 a/b - 1.0887 $(a/b)^2$*

For a/b < 0.5 the eta factor is nearly independent of the load level.

For a/b > 0.5 the eta factor is only constant for high load levels. This is due to the change of the plastic zone shape induced by geometrical effect.

The maximum relative error on the K_J value using this relation:

$$\eta = 0.9165 + 0.0297\ a/b - 1.0887\ (a/b)^2 \qquad (39)$$

is 4% for a/b<0.55 and 23% for 0.55<a/b<0.95.

And the mean relative error is 2% for a/b<0.55 and 9% for 0.55<a/b<0.95

Figure 32 shows the effect of the yield stress on the eta factor. The eta factor decreases with the load level and the yield stress.

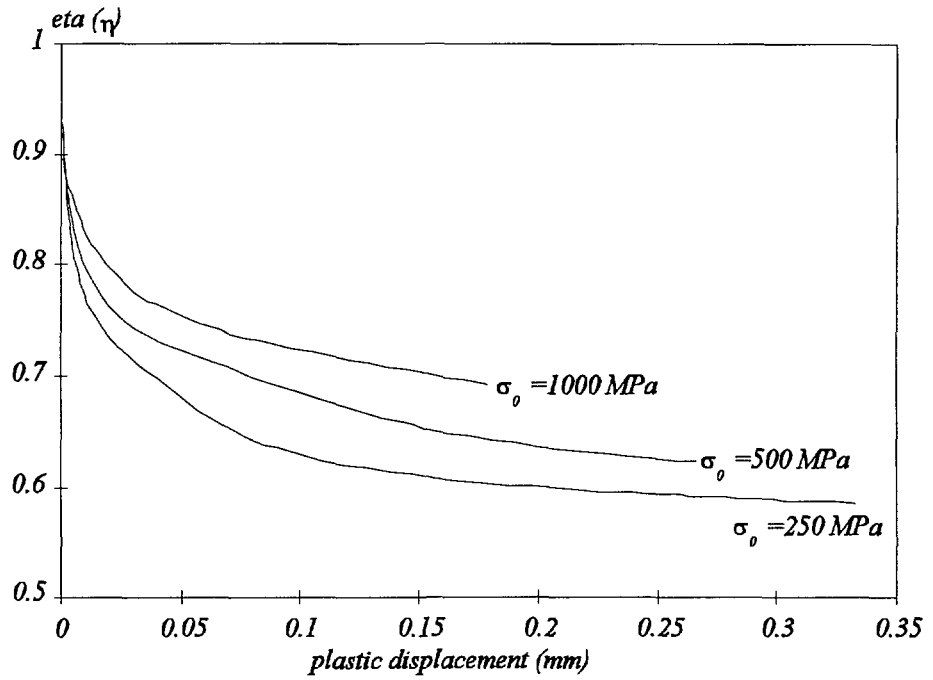

Figure 32 : *Eta factor as a function of the load level and the yield stress (a/b =0.5, n=0.1)*

To extend the validity of the eta factor for a/b>0.5 and high load levels, let's suppose that Equation 31 is valid for large plastic displacement ($\delta_{pl.} > \delta_{pl.init.}$). This hypothesis is supported by the fact that for high load levels the shape of the plastic zone does not change.

Now, the plastic part of the J-integral can be split in two parts:

$$J_{pl.} = \int_0^{\delta_{pl.init.}} \left(\frac{\partial P}{2\pi a\ \partial a}\right)_{\delta_{pl.}} d\delta_p + \int_{\delta_{pl.init.}}^{\delta_p} \left(\frac{\partial P}{2\pi a\ \partial a}\right)_{\delta_{pl.}} d\delta_{pl.} \tag{40}$$

An eta factor for high load levels is introduced:

$$J_{pl.} = J_{pl.init.} + \frac{\eta_{init.}}{2\pi a^2} \int_{\delta_{pl.init.}}^{\delta_p} P\ d\delta_{pl.} \quad \text{with} \quad \eta_{init.} = 2 + \frac{2\pi a}{F_2}\frac{\partial F_2}{\partial a} \tag{41}$$

The application of Equation 41 is less convenient than the conventional eta factor as it requires the determination of $\delta_{pl.init.}$ and $J_{pl.init.}$.

To summarise all the parameters characterising the eta factor, all parameters are written in a dimensionless manner:

$$\eta_{pl.} = \eta_{pl.}\left(\frac{E}{\sigma_0}, n, \frac{a}{b}, \frac{L}{b}, \frac{\delta_{pl.}}{b}\right) \tag{42}$$

- The E/σ_0 ratio influences the eta factor in the range of $205 < E/\sigma_0 < 820$ for a/b=0.5.

- The hardening exponent n does not influence the eta factor in the range of $0.05 < n < 0.2$ for a/b=0.5.

- The a/b ratio influences strongly the eta factor. Its influence can be modelled using the polynomial fit (see Equation 39) for $E/\sigma_0 = 420$.

- The L/b ratio does not influence the eta factor for $a/b < 0.65$ and $L/b > 4$ because the plastic zone size is always limited in the axial direction. For $a/b > 0.65$, the L/b effect on the eta factor is not studied.

- For $a/b < 0.45$, $\delta_{pl.}/b$ has no effect on the eta factor. For $a/b > 0.45$, $\delta_{pl.}/b$ has an effect on the eta factor for medium load levels ($\delta_{pl.}/b \approx 0.032$).

The analysis of the a/b ratio shows an optimal value $0.3 < a/b < 0.55$ to measure high fracture toughness without loss of triaxiality.

Good analytical approximate formulae to determine the J-integral were found for deep crack when $a/b < 0.3$.

For $0.4 < a/b < 0.7$, no accurate formulae are found and even the theory of the eta factor can not be applied successfully for medium load levels. It is thus recommended to use finite element calculation to simulate each experiment. If finite element computations are not available, the use of the polynomial eta factor (Equation 39) is recommended.

2.5 Path independence

The J-integral value is computed using two different methods available in the SYSTUS code: J2D based on Equation 13 and Jn based on Equation 16. To get a valid value, the J-integral should be path independent.

The J2D and Jn integral are plotted versus the radius of the path (see Figure 33) for different load levels.

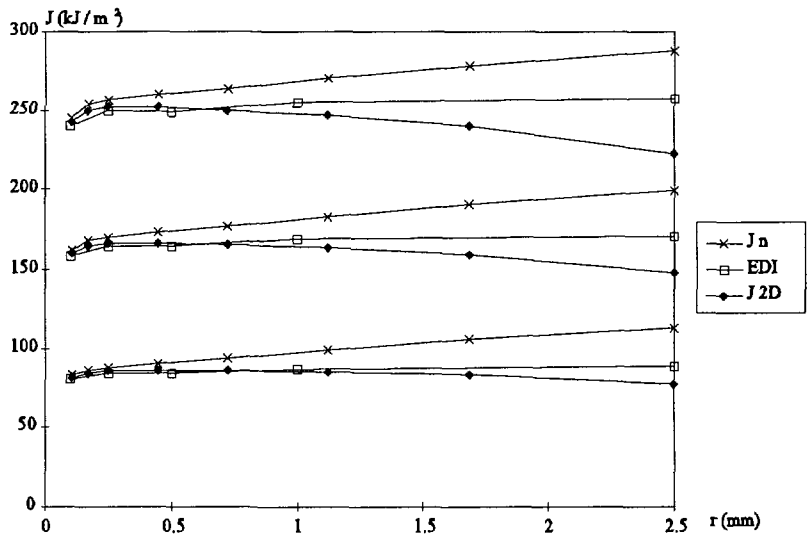

Figure 33 : *J-integral at different load levels for different paths (a/b = 0.5, n=0.1, E/σ_0=410)*

The path dependence of the Jn integral is clear (see Figure 33). This was also observed by [MUD-82, BER-81]. But none of these authors found an explanation. It is important to emphasize that all results [MUD-82, BER-81] were obtained with the same finite element code. So the validity of the method and its implementation is questionable.

The values obtained by J2D (Equation 13) are theoretically path dependent. In fact, the surface integral term (see Equation 15) increases when the path has a large radius. This explains the small decrease of the computed J integral (see Figure 33).

To obtain more reliable values, another method based on an exact formulation is developed and integrated into the SYSTUS code. The Equivalent Domain Integral is chosen, as it has already shown good results [MOR-91].

The formulation is based on an equation [MOR-91] derived for externaly cracked round bar and based on Equation 14:

$$J = \int_{\Omega} \left[\left(W \, \partial_1 q - \sigma_{\alpha\beta} \, \partial_\beta q \, \partial_\alpha u_1 \right) \frac{r}{a} + W \, q - \varepsilon_3 \sigma_3 \, q \right] d\Omega \qquad (43)$$

Where q is any continuous function with a value of one at the crack tip and zero at the border of Ω, all quantities are expressed in cylindrical coordinates.

The method is very attractive as:

- it requires only a surface integral and no path integral,
- the method is simple to integrate into a finite element code,
- the independence of J regarding the q function can be verified easily,
- the accuracy is assured as values are computed at the gauss points.

More details about the method and the code can be found in Annex 1.
Figure 33 shows that J-integral is nearly path independent and consequently all results are based on this method.

3 Comparison precracked bar versus precracked Charpy

The axisymmetric geometry is considered to be a high constrained geometry. This characteristic allows valid measures of the fracture toughness on smaller specimens. A possible way to detect a loss of constraint is to plot the stress ahead of the crack front in a dimensionless manner (see Equation 18). If the curves can not be superimposed, J is not the unique factor that characterises the loading. In this case an other parameter (Q factor or T stress) should be introduced [AND-95] to take into account the loss of constraint. The characterisation of the fracture toughness becomes more difficult and, generally, micro-mechanical models are used to avoid a two-parameter model of rupture. The present study is focused on the limit of the J-dominance for the precracked Charpy and the axisymmetric geometry.

In the present study, the ratio a/b, the hardening exponent and the E/σ_0 ratio are fixed to respectively a/b=0.5, n=0.1 and E/σ_0 =410 for both geometries. A large strain model is used to take into account large stain occurring in the blunting zone. A blunted initial mesh (see Figure 35) is used to avoid mesh distortion. Results are independent [IRS-96] of the initial radius when the crack tip opening displacement is six times greater than the initial blunting radius.

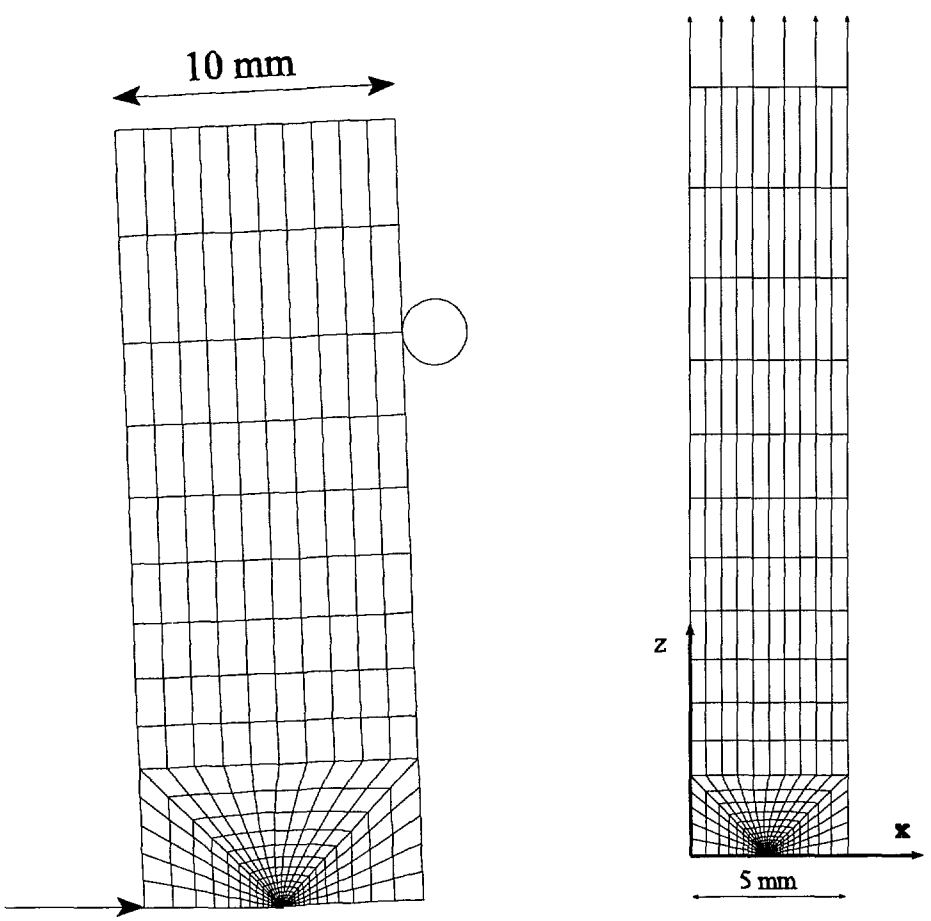

Figure 34 : *Mesh for the precracked Charpy and the circumferentially-cracked bar*

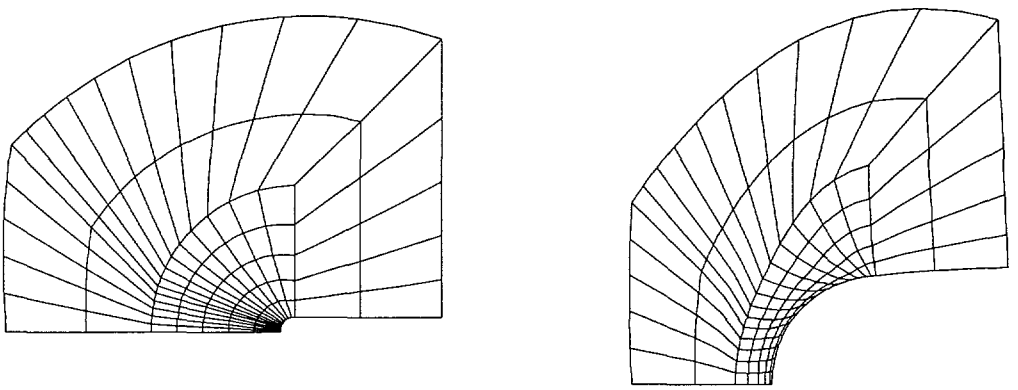

Figure 35 : *Crack tip mesh before and after deformation*

Figure 36 shows the CTOD versus the J-integral for both geometries. CTODr is the ratio between the actual CTOD and the CTOD of the initial mesh (CTODi). The slope of the theoretical line (0.5) is derived from the HRR solution [AND-95] under plane strain condition with n = 0.1 and E/σ_0 = 410. This HRR solution was obtained analytically by Hutchinson [HUT-68], Rice and Rosengren [RIC-68b] using a power law hardening material. The CTOD varies linearly with the J-integral and the slope is predicted accurately using small strain theory (HRR field).

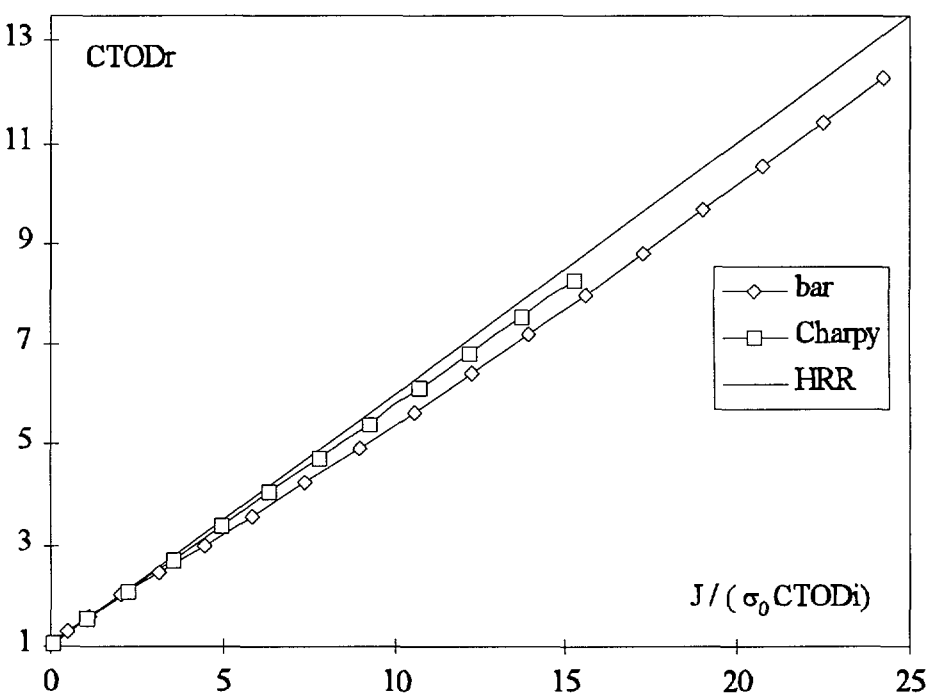

Figure 36 : *CTOD ratio versus J-integral*

Figures 37 and 38 show the opening stress ahead of the crack tip for the Charpy and the round bar.

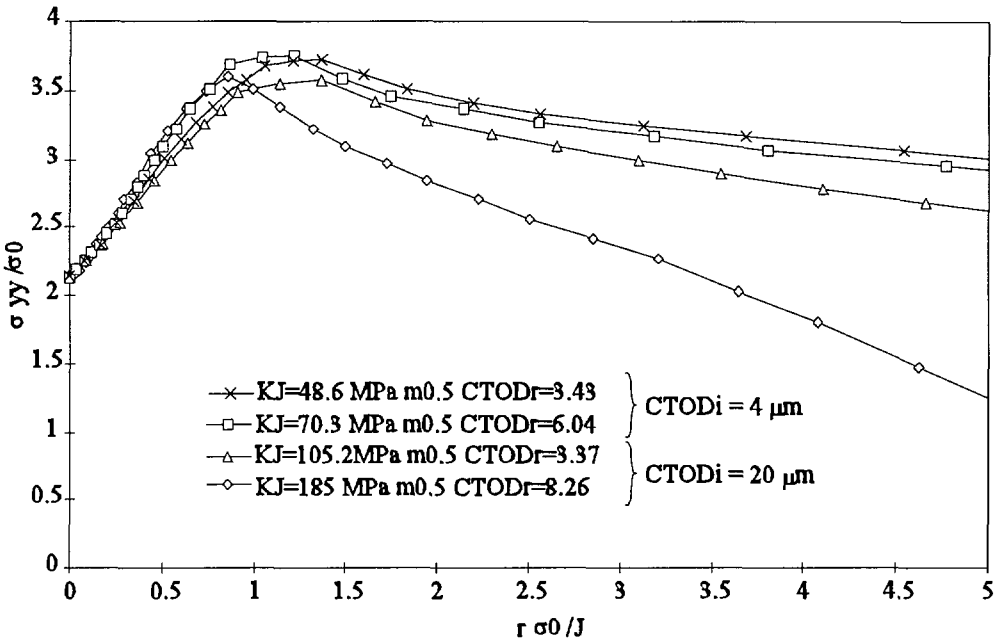

Figure 37 : *Opening stress in front of the crack tip (precracked Charpy)*

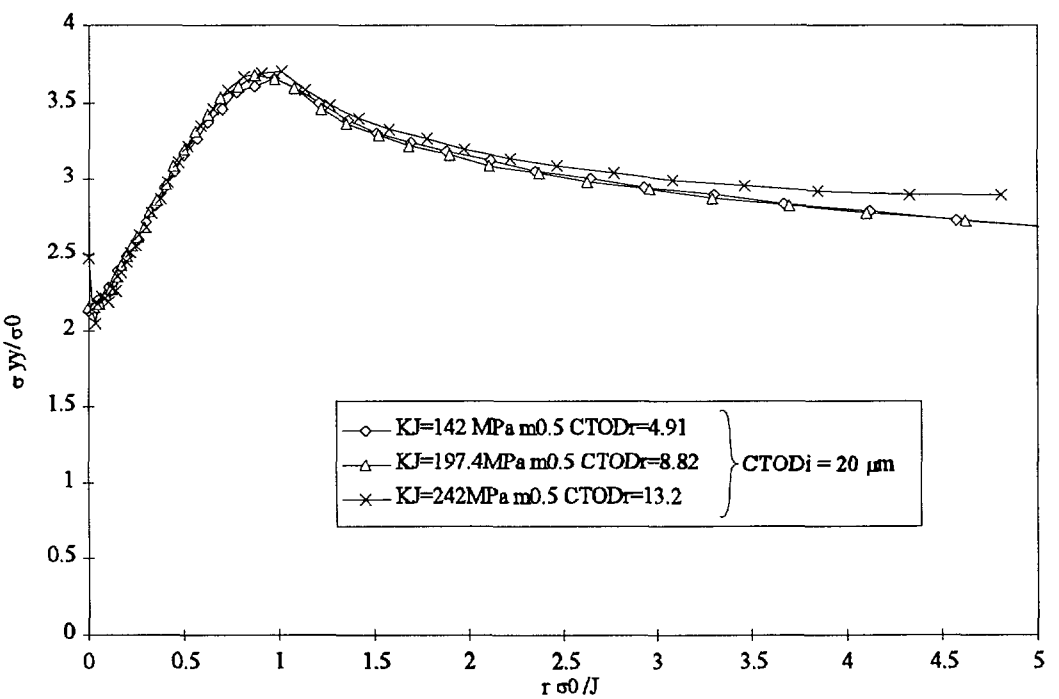

Figure 38 : *Opening stress in front of the crack tip (precracked bar)*

The opening stress distribution is independent of the load level for the precracked bar. For the Charpy specimen and for a stress intensity factor greater than 100 MPa $m^{0.5}$, the stress decreases drastically indicating clearly a loss of constraint.

Figures 39 and 40 show the triaxiality ratio (hydrostatic stress to the equivalent Von Mises stress) ahead of the crack tip for the Charpy and the bar respectively.

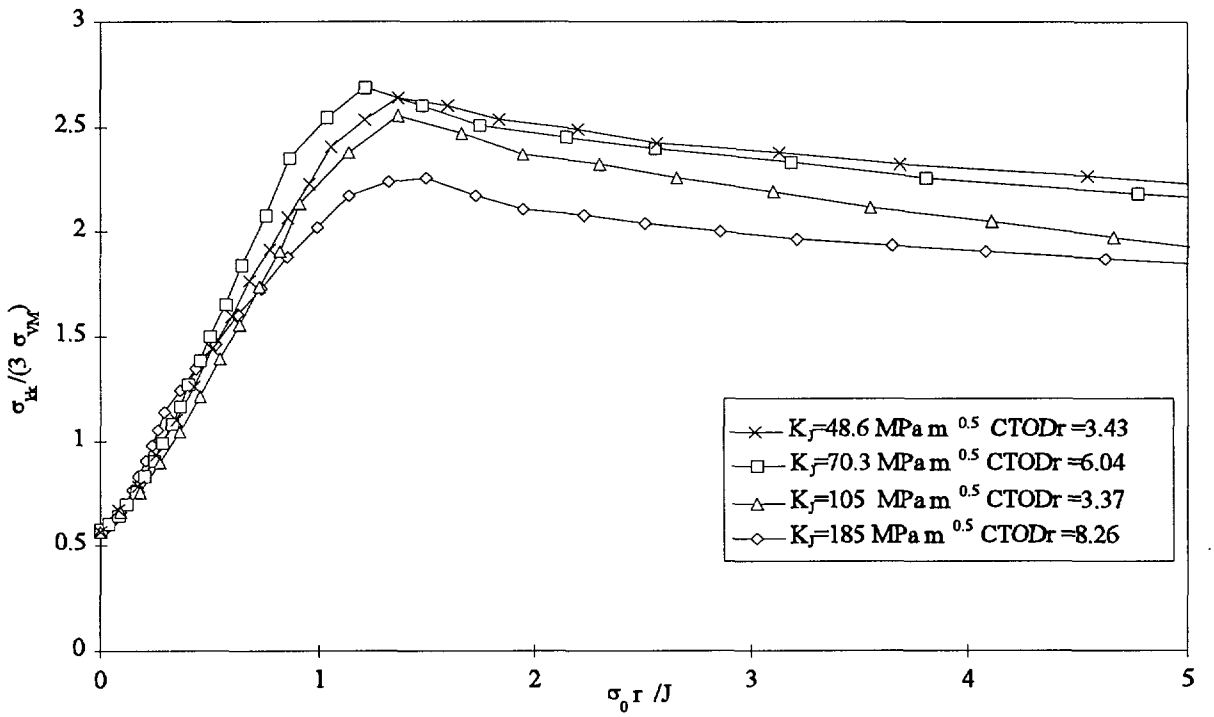

Figure 39 : *Triaxiality in front of the crack tip for the Charpy specimen*

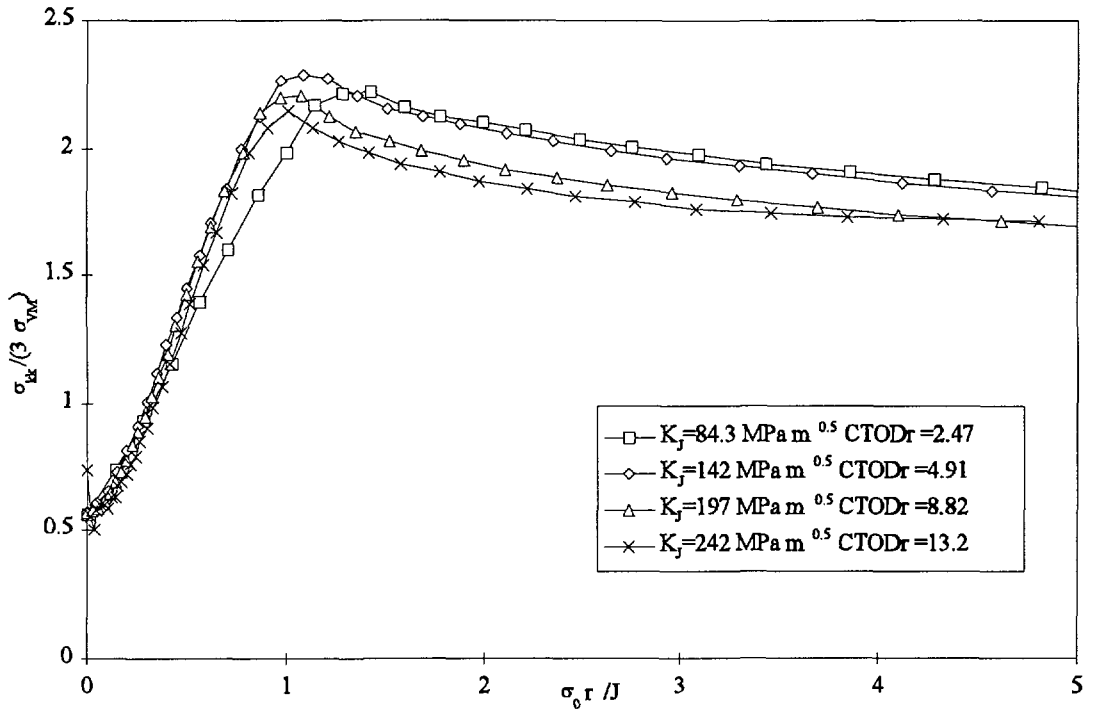

Figure 40 : *Triaxiality in front of the crack tip for the cracked bar*

For $r\sigma_0/J< 1$ in the large strain zone, the triaxiality ratio increases from 0.6 to 2. The loss of triaxiality at the crack tip is due to the free surface. The theoretical value of the triaxiality at the crack tip in a plane strain configuration is 0.577 [MOR-91], in close agreement with our results.

In the cracked round bar, for $K_J<142$ MPa $m^{0.5}$ and for CTODr > 3, the triaxiality remains constant. For higher K_J values, the triaxiality decreases slowly, resulting in a loss of constraint.

On the other hand, this loss of constraint appears earlier for the precracked Charpy K_J=70 MPa $m^{0.5}$. Moreover for this geometry, three-dimensional effects can also induce a loss of constraint.

In conclusion, the comparison of the two geometries shows that

- the axisymmetric geometry is close to plane strain condition,
- the cracked round bar has a lower triaxiality ratio, but this triaxiality is maintained up to higher K_J levels.

To verify the validity of the finite element calculations performed here, a comparison to Moran's results [MOR-91] is made.

The geometrical parameters and material properties are the same as Moran's one, namely:

- a/b = 0.25,
- n = 0.1,
- σ_0/E = 0.002,
- L/b = 4,
- CTODi /a = 2 10^{-3}.

The load level is such that: σ_0 a/J = 140, the J-integral was evaluated by Moran using the equivalent domain integral.

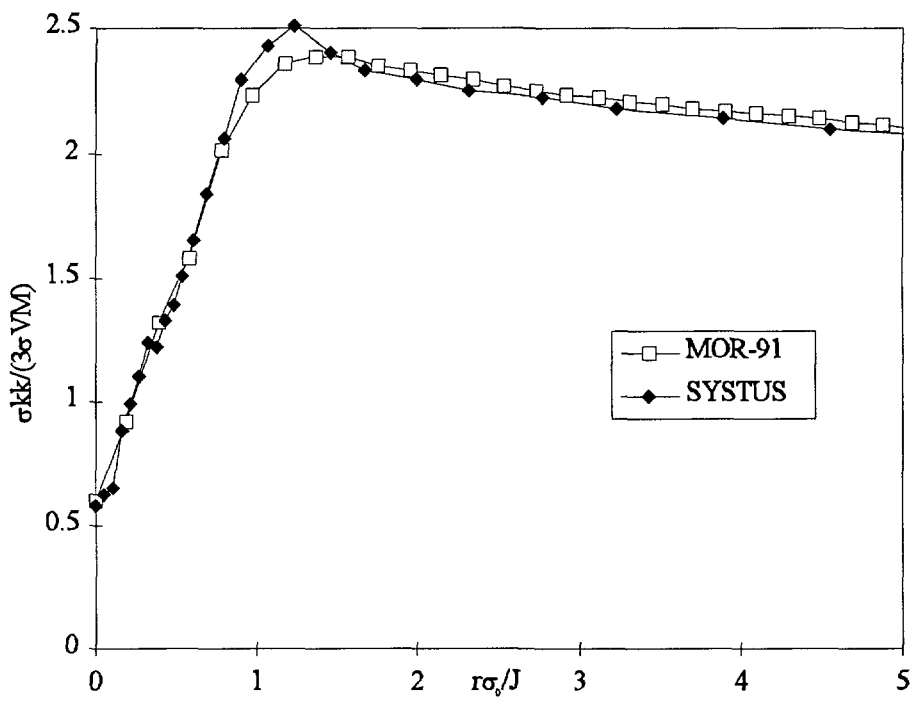

Figure 41 : *Triaxiality in front of the crack tip for the cracked bar*

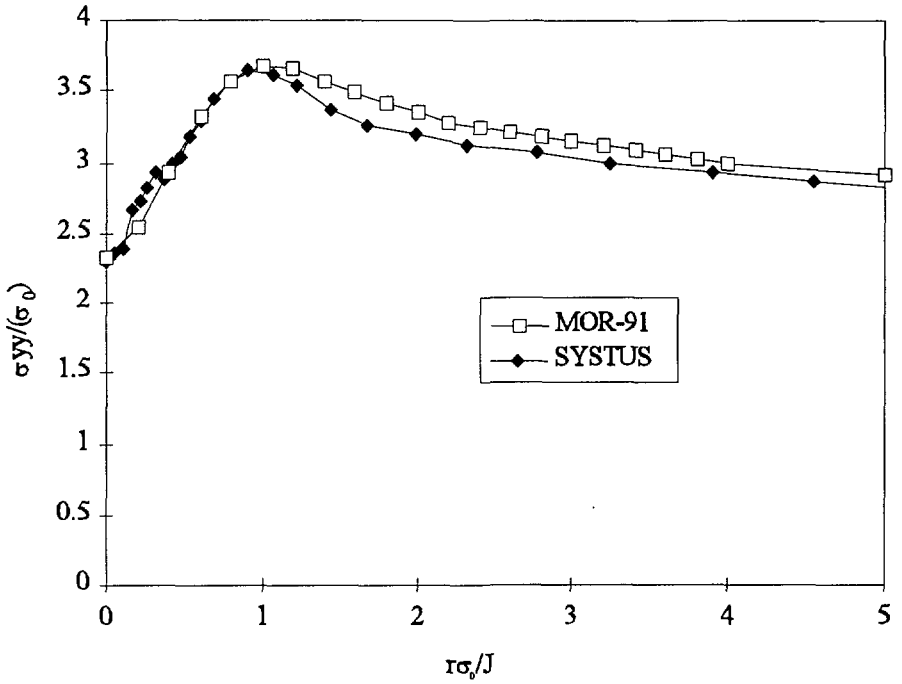

Figure 42 : *Opening stress in front of the crack tip for the cracked bar*

Figures 41 and 42 show a very good agreement with Moran's result as well for the opening stress distribution as for the triaxiality ahead of the crack tip. The validity of finite element calculations presented in this report is thus verified.

4 Conclusions and further investigations

4.1 Fracture toughness

Different authors established a domain of validity for elastic fracture toughness measurement on circumferentially-cracked round bar. All authors agree fairly well in the range of interest $0.4<a/b<0.6$. The established condition is 6 times less severe than with standard bending specimens.

For elastic plastic fracture mechanics, literature suggests different approximate formulae but the domain of validity and the accuracy are not always mentioned. Therefore, several finite element calculations were performed showing that within the tested range:

- the strain hardening exponent does not affect the accuracy of the different formulae,
- the ratio σ_0/E, the load level and the a/b ratio affect the accuracy of the different formulae.

The recommended formulae for:

- $a/b<0.35$ are Itoh, Rice and Neale equations (maximum 10% error),
- $0.35<a/b<6.5$ is Neale (maximum 30% error),
- $a/b>0.65$ no accurate formula is found (except for low J levels).

To improve the accuracy, the theory of the eta factor is successfully applied in nearly all the a/b range and for high or low load levels. However, some further work is required to extend the validity and the accuracy of the proposed expression for the eta factor.

In the same time, this analysis suggests an optimal value of $0.3<a/b<0.55$ to measure high fracture toughness.

To compute the J-integral using finite element results for axisymmetric configurations, current available methods are not satisfactory. The Equivalent Domain Integral (EDI) is consequently implemented and gives complete satisfaction.

4.2 Comparison cracked bar versus precracked Charpy

Comparison of the precracked Charpy and the circumferentially-cracked bar shows that

- the axisymmetric geometry is close to plane strain condition,
- the cracked round bar has a slightly lower triaxiality ratio, but this triaxiality is maintained up to higher K_J levels allowing valid measures of the fracture toughness on smaller specimens.

5 References

[AND-95] Anderson T.L. "Fracture mechanics fundamentals and applications", CRC Press second edition, London, pp. 1-680, 1995

[AST-90] A.S.T.M. "Annual book of ASTM standards" Section 3 Metals test Methods and analytical procedures, Printed in Easton, MD, USA, 1990

[BEN-73] Benthem J.P. and Koiter W.T. "Asymptotic approximations to crack problems", in Methods of Analysis and Solutions of Crack Problems (Edited by G.C. Shi), chap. 3, pp. 131-178, Noordhoft International Publishing, Groningen, 1973

[BER-77] Bergkvist H. and Huong G.L. "J-integral Related quantities in axisymmetric cases", Int. Journ. of Fracture 13, pp.556-558, 1977

[BER-81] Beremin F.M. "Calculation and experiment on axisymmetrically cracked tensile bars: prediction of initiation, stable crack growth and instability", 6th SMIRT, Paris 1981

[BRO-76] Broberg K.B. "On Determination of the J-integral for paths close to a crack-tip in cases of axial symmetry", report SM 76-9, Graduate Aeronautical Laboratories, California Institute of Technology, Pasadena, Calif., 1976

[BUD-73] Budiansky B. and Rice J.R. "Conservation laws and energy-release rates", Journal of Applied Mechanics, pp.20-203, march 1973

[HUT-83] Hutchinson J.W. "Singular behaviour at the end of a tensile crack in a hardening material", Journal of the Mechanics and Physics of Solids, Vol. 16, pp 13-31, 1968

[HUT-83] Hutchinson J.W. "Fundamentals of the phenological theory of nonlinear fracture mechanics", Journal of Applied Mechanics, Vol. 50, pp. 1042-1051, december 1983

[IBR-87] Ibrahim R.N. and Stark H.L. "Validity requirements for fracture toughness measurements obtained from small circumferentially notched cylindrical specimens", Engineering Fracture Mechanics Vol. 28, No. 4, pp. 455-460, 1988

[IRS-96] I.R.S.I.D. "Mise en place d'une méthodologie simplifiée pour utiliser des critères locaux de rupture", Internal report, RE 96.03 Maizières-lès-Metz, France, February 1996

[ITO-88] Itoh Y.Z., Murakami T. and Kashiwaya H. "Approximate formulae for estimating the J-integral of a circumferentially cracked round bar under tension or tortion", Engineering Fracture Mechanics Vol. 31, No. 6, pp 967-975, 1988

[LUC-90] Lucon E. "Fracture toughness testing using small cylindrical specimens with ring-shaped cracks", ECF 8 Fracture Behaviour and design of Materials and Structures", Fracture Behavior and Design of Material and Structures, Proceeding of ECF8, 8th Biennial European Conference on fracture, D. Firrao, Ed., Vol. II, EMAS, London, pp. 1077-1082, 1990

[LUC-92] Lucon E. "Lucon E. "Cylindrical specimens for evaluating a serviced component's fracture toughness properties", presented at the Ninth European Conference on fracture ECF9, Varna (Bulgaria), 21-25 September 1992

[MOR-87] Moran B. and Shih S., "Crack tip and associated domain integrals from momentum and energy balance", Engineering Fracture Mechanics, Vol. 27, No. 6, pp. 615-642, 1987

[MUD-82] Mudry F. "Etude de la rupture ductile et de la rupture par clivage d'aciers faiblement allies", thesis, University of Compiegne, France, march 1982

[NEA-95] Neale B.K. "The analitycal fracture behaviour of a bar in tension containing a circumferential edge crack", Internal Report TEMP/REP/0131/94, Nuclear Electric, England, January 1995

[PAR-80] Paris P.C. Ernst H. and Turner C.E. "A J-integral approach to devlopment of eta factors", Fracture Mechanics: Twelfth Conference, ASTM STP 700, American Society for Testing and Materials, pp. 338-351, 1980

[RIC-68a] Rice J.R. "A Path independent integral and approximate analysis of strain concentration by notches and cracks", Journal of applied Mechanics, pp 379-386, june 1968

[RIC-68b] Rice J.R. and Rosengren G.F. "Plane strain deformation near a crack tip in a power-law hardening material", Journal of the Mechanics and Physics of Solids, Vol. 16, pp 1-12, 1968

[RIC-73] Rice J.R., Paris P.C. and Merkle J.G."Some further results of J-integral analysis and estimates", ASTM STP 536, pp. 231-245, 1973

[SHE-82] Shen Wei, Zhao Tingshi, Gao Daxing, Li Dunkang, Li Poliang and Qui Xiaoyun "Fracture toughness measurement by cylindrical specimen whith ring-shaped crack", Engineering Fracture Mechanics Vol. 16, No. 1, pp. 69-82, 1982

Annex 1 The Equivalent Domain Integral (EDI)

A1.1 Theoretical aspects

Some more explanations are needed to understand the practical implementation of Equation A1 in a finite element code.

$$J = \int_{\Omega} \left[(W\, \partial_1 q - \sigma_{\alpha\beta}\, \partial_\beta q\, \partial_\alpha u_1)\, \frac{r}{a} + W\, q - \varepsilon_3 \sigma_3\, q \right] d\Omega \tag{A1}$$

Where q is any continuous function with a value of one at the crack tip and zero at the border of Ω.

First, the discretisation of Equation A1 into elements gives:

$$J = \sum_{elements\ \in\ \Omega} \sum_{Gauss\ points} \left[(W\, \partial_1 q - \sigma_{\alpha\beta}\, \partial_\beta q\, \partial_\alpha u_1)\, \frac{r}{a} + W\, q - \varepsilon_3 \sigma_3\, q \right] \omega \left| \frac{\partial x}{\partial \xi} \right| \tag{A2}$$

Where ω is the Gauss weight of the Gauss point and ξ the isoparametric coordinates.

The displacement variation along the direction 1 is calculated at Gauss point using the variation of the shape function and the nodal displacement of the element:

$$\frac{\partial u_2}{\partial x_1} = \frac{\partial N_2}{\partial x_1}\, u_{2,\ nodal} \tag{A3}$$

The first chosen q function is linear:

$$q = \begin{cases} 1 - \dfrac{\|x - x_0\|}{R_0} & if\ \|x - x_0\| \le R_0 \\ 0 & if\ \|x - x_0\| > R_0 \end{cases} \tag{A4}$$

Where $\mathbf{x}_0$ is the position of the crack tip and R_0 a user parameter controlling the area size of integration.

The derivation of q function is obtained very easily:

$$\partial_i q = \begin{cases} -\dfrac{x_i - x_{i0}}{\|x - x_0\|\, R_0} & if\ \|x - x_0\| \le R_0 \\ 0 & if\ \|x - x_0\| > R_0 \end{cases} \tag{A5}$$

A second q function giving slightly better results (i.e. a more constant value) is chosen:

$$\begin{cases} 1 - 3\left(\dfrac{\|x - x_0\|}{R_0}\right)^2 + 2\left(\dfrac{\|x - x_0\|}{R_0}\right)^3 & if\ \|x - x_0\| \le R_0 \\ 0 & if\ \|x - x_0\| > R_0 \end{cases} \tag{A6}$$

The derivation of q function is:

$$\partial_i q = \begin{cases} -6\,\dfrac{x_i - x_{i0}}{R_0^2} + 6\,\dfrac{x_i - x_{i0}\,\|x - x_0\|}{R_0^3} & \text{if } \|x - x_0\| \le R_0 \\ 0 & \text{if } \|x - x_0\| > R_0 \end{cases} \tag{A7}$$

For points near to the crack tip and near the outer diameter the variation of the q function is null (Equation A7). Thus, it decreases the importance of points near the crack tip (blunting zone) and near the outer region (better continuity between inside and outside region). The path independence is always better than the linear function, thus the cubic q function is strongly advised.

A1.2 Code for the EDI

The code is in SIL language. This is an interpreted language provided with the SYSTUS code allowing direct access to the data base.

```
//J integral by the equivalent domain integral for an half axisymmetric geometry
//*****************************************************************************

//version4 1/4/96
//***************


//declaration of variable
//***********************
variable i,j,k,l;     // loop counter
variable ncard;       // number of card
variable nelem;       // number of element
variable nbgauss;     // number of Gauss point
variable ncont;       // number of path
variable j_externa;   // external number of an element
variable nodes[8];    // nodes of an element
list list_card;       // list of cards number
list xlist_displ[2]; // list of displacements for all nodes of an element
list xlist_coor[3];  // list of Gauss coordinate for an element
list xlist_weight;   // list of Gauss weight
list form[8];         // list shape function value for an element at Gauss point
list det;             // list Jacobian determinant for an element at Gauss point
list dv[3,8];         // list of shape function derivate for an element
list rot[3,3];        // list of rotation matrix
variable ac[200];     // stress vector
variable dum,dum1;    // temporary variable
variable idum,sdum$;  // temporary variable
variable dumv[7];     // temporary variable
variable tipx,tipy;   // x and y coordinate of the crack tip
list rayon;           // list of radius controling the integration size
list xinteg[7];       // list of integral term for all radius
                      // and for the two q function
variable a;           // radius of the ligament;
variable da;          // surface element
variable w;           // total energy density
variable dvdx;        // variation of v displacement versus x coordinate
variable q;           // q function
variable dqdx;        // q derivate along the x axis
variable dqdy;        // q derivate along the y axis
variable x,y;         // x and y coordinate of a Gauss point


//initialization
//**************
initialize_list(list_card);
ncard = number_of_tran_maps(1);
list_card = tran_maps(1);
nelem = code_systus("mmaxi");


//read data (tipx,tipy,ncont,rayon)
//*********************************
kfile = open_file("'p1'","read");  //p1 is the name of the file

write_screen("\n%s\n","   J-integral by the equivalant domain integral (EDI)");
write_screen(  "%s\n","   for an half axisymmetric geometry");
write_screen("%s\n\n","   version 4 : 1/4/96");

read_file(kfile,"%s",sdum$);
read_file(kfile,"%s",sdum$);
read_file(kfile,"%f",tipx);

read_file(kfile,"%s",sdum$);
read_file(kfile,"%f",tipy);

write_screen("coordinate of the crack tip X = %f ",tipx," Y = %f\n\n", tipy);

read_file(kfile,"%s",sdum$);
read_file(kfile,"%d",ncont);
```

```
initialize_list(rayon);
initialize_list(xinteg);

write_screen("number of path %d\n",ncont);
for(i=1;i<=ncont;i=i+1)
{
   read_file(kfile ,"%f",dum);
   write_screen("radius %d ",i, "= %f\n",dum);
   rayon#=dum;
   xinteg#=dumv;
}
for(i=1;i<=ncont;i=i+1)
{
   rayon#=rayon[i];
   xinteg#=dumv;
}
write_screen("%s\n","");
//end read data

write_screen("\n%s","    J   = 2 * (   J1       - J2       - J3       - J4");
write_screen("%s\n","       - J5       + J6       - J7)");

for(i=2;i<=ncard;i=i+1)          // loop on cards
{
   for(j=1;j<=2*ncont;j=j+1)     // loop on path and q function
                                 // (linear and cubic)
   {
       for(k=1;k<=7;k=k+1)
       {
          xinteg[j,k]=0;
       }
   }
   for(j=1;j<=nelem;j=j+1)       // loop on element
   {
      j_external=int_element_ext_number(j);
      if(element_code(j_external)==2008)
      {
         initialize_list(xlist_displ);
         initialize_list(xlist_coor);
         initialize_list(xlist_weight);
         initialize_list(form);
         initialize_list(det);
         initialize_list(dv);
         initialize_list(rot);
         nodes = nodes_of_element(j_external);
         xlist_displ = trans_node_displacement(list_card[i],nodes);
         element_integration(j_external,xlist_coor,xlist_weight);
         shape_function(j_external,xlist_coor,form,det,dv,rot);
         ac=trans_element_stress(list_card[i],j_external);
         nbgauss=length(xlist_coor);

// dvdx da
//********
         for(k=1;k<=nbgauss;k=k+1)
         {
            dvdx=0;
            for(l=1;l<=8;l=l+1)
            {
               dvdx = dvdx + dv[k,l,1] * xlist_displ[l,2];
            }
            ac[30+40*k]=dvdx;
            ac[31+40*k]=xlist_weight[k] * det[k];
         }
//end dvdx da


         for(k=1;k<=2*ncont;k=k+1)
         {

//q function and derivate
//***********************
            for(l=1;l<=nbgauss;l=l+1)
            {
               x=ac[22+40*l];
               y=ac[23+40*l];
               dist=sqrt((x-tipx)*(x-tipx)+(y-tipy)*(y-tipy));
               if(dist>rayon[k])
```

```
                {
                   ac[32+40*l]=0;
                   ac[33+40*l]=0;
                   ac[34+40*l]=0;
                }
                else
                {
                   if(k<=ncont)
                   {
                      // linear function
                      ac[32+40*l]= 1.- dist % rayon[k];
                      ac[33+40*l]= -(x-tipx)%(rayon[k]*dist);
                      ac[34+40*l]= -(y-tipy)%(rayon[k]*dist);
                   }
                   else
                   {
                      // cubic function
                      dum= dist % rayon[k];
                      ac[32+40*l]= 1.- 3 * dum*dum + 2*dum*dum*dum ;
                      dum1 = (x-tipx)%(rayon[k]*dist);
                      ac[33+40*l]= (-6*dum+6*dum*dum)*dum1;
                      dum1=(y-tipy)%(rayon[k]*dist);
                      ac[34+40*l]= (-6*dum+6*dum*dum)*dum1;
                   }
                }
             }
//end q function


//addition and output result to screen
//************************************
             for(l=1;l<=nbgauss;l=l+1)
             {
                 a= tipx;
                 x =   ac[22+40*l];
                 y =   ac[23+40*l];
                 w =   ac[21+40*l];
                 sigx= ac[1+40*l];
                 sigy= ac[2+40*l];
                 sigxy=ac[3+40*l];
                 sigz= ac[4+40*l];
                 epsix=ac[5+40*l];
                 epsiy=ac[6+40*l];
                 epsiz=ac[8+40*l];
                 dvdx= ac[30+40*l];
                 q=    ac[32+40*l];
                 dqdx= ac[33+40*l];
                 dqdy= ac[34+40*l];
                 da=   ac[31+40*l];
xinteg[k,1]=xinteg[k,1]+             w * dqdx * x * da % a;
xinteg[k,2]=xinteg[k,2]+  sigx * epsix * dqdx * x * da % a;
xinteg[k,3]=xinteg[k,3]+ sigxy * epsix * dqdy * x * da % a;
xinteg[k,4]=xinteg[k,4]+ sigxy * dvdx  * dqdx * x * da % a;
xinteg[k,5]=xinteg[k,5]+  sigy * dvdx  * dqdy * x * da % a;
xinteg[k,6]=xinteg[k,6]+ w * q * da % a;
xinteg[k,7]=xinteg[k,7]+ epsiz * sigz * q * da % a;
             }
//end addition

          }
       }
   }
   write_screen("CARD %d\nlinear\n",list_card[i]);
   for(j=1;j<=2*ncont;j=j+1)
   {
      if(j==ncont+1)   write_screen("%s\n","cubic");
      dum= xinteg[j,1]-xinteg[j,2]-xinteg[j,3];
      dum = dum-xinteg[j,4]-xinteg[j,5]+xinteg[j,6]-xinteg[j,7];
      write_screen("%10f ",(2*dum) };     // 2 factor due to x symmetry
      write_screen("%10f ",xinteg[j,1],"%10f ",xinteg[j,2]);
      write_screen("%10f ",xinteg[j,3],"%10f ",xinteg[j,4]);
      write_screen("%10f ",xinteg[j,5],"%10f ",xinteg[j,6]);
      write_screen("%10f\n",xinteg[j,7]);
   }
   write_screen("%s\n","");
}
```

A1.3 Example of use

Input data file (name of the file "axi.dat")

```
definition
 test of the equivalent integral method
option two-dimensional axisymmetric
two-dimension generate 1
nodes
 1/             0       0
 2/             5       0
 3/             5       5
 4/             0       5
edge
 1/             1       2       4
 2/             2       3       4
 3/             3       4       4
 4/             4       1       4
elements
 1/     2 3 4 1
verify
renu iter 30
materials
 E 205000 nu 0.3 yield 500 slope -3 model 2 integ 2
constraints
 line node 1 4 /ux
 node 34 to 37     /uy
 node 1 /ux uy
 line node 4 3 /uy
load
1 displacement fixed
 line node 4 3 /uy=1 FT11
table
  3/1
 0.00243902 500.000
 0.00462178 533.003
 0.00842792 566.005
 0.01485392 599.008
 0.02539561 632.010
 0.04224913 665.013
 0.06857530 698.016
 0.10884246 731.018
 0.16926544 764.021
 0.25836116 797.023
 0.38764439 830.026
 0.57249070 863.029
 0.83319739 896.031
 1.00000000 912.533
 11/1 0 0 10 10
return

trans non line stat
beha plastic update
algo iter 150 opti 19 bfgs
time init 0
 0.04 step 0.01 /store 2
return

save data tran 1
```

Input data for the Equivalent Domain Integral (name of the file "arc.edi")

```
tip x 2.5 y 0
ncont 4
1
1.5
2
2.5
```

Command to begin the computation

```
assi axi.dat
read
lang
@edi arc.edi
```

Results

```
 J-integral by the equivalant domain integral (EDI)
   for an half axisymmetric geometry
   version 4 : 1/4/96

coordinate of the crack tip X = 2.500000  Y = 0.000000

number of path 4
radius 1 = 1.000000
radius 2 = 1.500000
radius 3 = 2.000000
radius 4 = 2.500000
```

J = 2 * (	J1	- J2	- J3	- J4	- J5	+ J6	- J7)
CARD 2							
linear							
11.610868	-0.312358	-0.136867	0.099769	-1.597749	-3.670642	0.782149	-0.030154
15.530169	0.120600	-0.202978	0.158264	-1.249479	-4.975806	1.317843	-0.056643
17.111197	0.351341	-0.208643	0.173987	-1.013464	-5.184717	1.892805	-0.078616
17.430595	0.424417	-0.192336	0.173992	-0.817769	-4.909182	2.448437	-0.097149
cubic							
15.846832	-0.444623	-0.191890	0.140980	-2.253659	-5.175679	0.854842	-0.032950
17.154560	0.047562	-0.166806	0.230582	-1.350801	-5.861323	1.325681	-0.055690
18.114738	0.372822	-0.198603	0.222847	-0.968363	-5.801710	1.860482	-0.078236
18.012596	0.520367	-0.205315	0.189549	-0.732006	-5.218066	2.420183	-0.099911
CARD 4							
linear							
29.346375	-1.214884	-0.467017	0.298949	-3.836773	-9.915735	1.836361	-0.131135
40.088390	-0.501831	-0.730291	0.473245	-3.080193	-13.857663	3.126122	-0.225004
44.644062	0.002370	-0.821013	0.504061	-2.493611	-14.643855	4.546392	-0.318850
45.678177	0.199827	-0.772537	0.482746	-1.998691	-14.023034	5.925795	-0.401951
cubic							
40.224972	-1.736509	-0.654141	0.424613	-5.435186	-14.037359	2.003840	-0.143081
44.645378	-0.686884	-0.623461	0.692467	-3.350525	-16.371563	3.130877	-0.225614
47.505974	-0.020309	-0.768077	0.654813	-2.439660	-16.463457	4.443102	-0.313811
47.234196	0.358263	-0.817636	0.546390	-1.833991	-14.915582	5.832806	-0.405210

Command to stop SYSTUS

```
end
end
```